A comprehensive single-cell atlas of three centenarian cohorts unveils unique natural killer cell signatures and enhanced mutual interactions among peripheral immune cells

Bin Wang,[a,b,i] Zehao Zhang,[a,i] Qing Ouyang,[b] Min Zhang,[b] Mingda Duan,[c] Hongyan Hu,[d] Qingtao Zhang,[b] Xinye Jin,[a] Jie Zhang,[a] Qing Luo,[a] Ding Sun,[a] Hao Li,[a] Zeyu Qu,[a] Xiangmei Chen,[a,b,***] Zhifeng Gu,[e,**] and Yizhi Chen[a,b,f,g,h,*]

[a]Department of Nephrology, Hainan Hospital of Chinese PLA General Hospital, The Hainan Academician Team Innovation Center, Sanya, 572013, China
[b]Senior Department of Nephrology, Chinese PLA General Hospital, State Key Laboratory of Kidney Diseases, National Clinical Research Center for Kidney Diseases, Beijing, 100853, China
[c]Department of Anesthesiology, Hainan Hospital of Chinese PLA General Hospital, Sanya, 572013, China
[d]Department of Laboratory Medicine, Hainan Hospital of Chinese PLA General Hospital, Sanya, 572013, China
[e]Research Center of Clinical Medicine, Research Center of Gerontology and Longevity, Key Laboratory of Immunology, Department of Rheumatology, Affiliated Hospital of Nantong University, Nantong University, Nantong, 226001, China
[f]The Second School of Clinical Medicine, Southern Medical University, Guangzhou, 510515, China
[g]Sanya Nephrology Medical Quality Control Center, Sanya, 572013, China
[h]Hainan Medical University, Haikou, 571199, China

eBioMedicine
2025;120: 105922
Published Online xxx
https://doi.org/10.1016/j.ebiom.2025.105922

Summary

Background Centenarians are considered as an optimal population for studying healthy ageing. However, immune features associated with super longevity have only been investigated in a few small studies using a single research method.

Methods In this study, single-cell RNA sequencing (scRNA-seq), mass cytometry, and flow cytometry analysis were used to analyse the immune feature of peripheral blood mononuclear cells (PBMCs) from 17 centenarians (CENs), 9 of their offsprings (COs), and 14 of their offsprings' spouses or neighbours (controls, CTs) from Lingao County of China. scRNA-seq data from the other two cohorts were downloaded from public databases.

Findings Comprehensive analysis of 31 CENs, 17 COs, and 26 CTs from these three cohorts revealed decreased percentages of B cells and $CD4^+$ T cells and an increased percentage of natural killer (NK) cells in PBMCs from CENs, compared with CTs. Moreover, NK cells from CENs exhibited relatively "young" signatures, including cell subset distribution and key membrane receptor expression. Enhanced RUNX3 expression in NK cells was observed in CENs, with reinforced interactions between NK and T cells, which promoted T cell function by modulating MHC-I, CD99 and MIF signalling.

Interpretation CENs exhibit unique immunological features, especially NK cells with young protein expression signatures and immune functions.

Funding This study was funded by the Sanya Science and Technology Innovation Special Project (No. 2022KJCX02), National Natural Science Foundation of China (No. 32141005, 82270769), Specific Research Fund of the Innovation Platform for Academicians of Hainan Province, and National Key Research and Development Program of China (Nos. 2022YFC3602900, 2022YFC3602902, 2022YFC3602903).

*Corresponding author. Department of Nephrology, Hainan Hospital of Chinese PLA General Hospital, Sanya, 572013, China.
**Corresponding author. Department of Rheumatology, Affiliated Hospital of Nantong University, Nantong University, Nantong, 226001, China.
***Corresponding author. Senior Department of Nephrology, Chinese PLA General Hospital, Beijing, 100853, China.
E-mail addresses: yizchen@126.com (Y. Chen), guzf@ntu.edu.cn (Z. Gu), xmchen301@126.com (X. Chen).
[i]These authors contributed equally to this article.

Keywords: Centenarians; PBMCs; Single-cell RNA sequencing; Mass cytometry; Immune remodelling

Research in context

Evidence before this study

Centenarians are an established model of successful and healthy ageing. Previous research on centenarians' immune systems has been limited to small-scale studies using a single methodology, such as flow cytometry or targeted gene expression analyses. However, these studies lacked comprehensive multi-omics integration and validation across diverse cohorts.

Added value of this study

This study integrated scRNA-seq, mass cytometry, and flow cytometry to analyse PBMCs from 31 CENs, 17 COs, and 26 CTs across three cohorts (Lingao, Rugao, and Japan) to generate a multi-omics atlas of centenarian immune status. Through comprehensive analysis, we showed that CENs possess NK cells with "young" signatures and enhanced cytotoxicity linked to RUNX3 upregulation. Reinforced NK cell-T cell interactions via the MHC-I and MIF pathways promoted T cell function in CENs. The study overcomes the limitations of prior studies by combining high-resolution single-cell data with functional assays, offering a unified model of immune health in extreme ageing.

Implications of all the available evidence

Our findings, combined with existing evidence, redefine healthy immune ageing by demonstrating that centenarians maintain cytotoxic and regulatory balance through unique NK and T cell adaptations. For researchers, our study establishes a framework for exploring immune resilience, emphasising multi-omics approaches. For clinicians, targeting the identified pathways (RUNX3, MHC-I, or MIF) could help delay age-related immune decline, potentially reducing susceptibility to infections, cancer, and chronic inflammation.

Introduction

In recent decades, the average lifespan has increased considerably because of scientific and medical advancements. One in eleven people in the world is over the age of 65 years, and this ratio will rise rapidly to one in six (16%) by the 2050s, according to the United Nations.[1] Unfortunately, the increased ageing of the global population is accompanied by a growing number of age-related diseases, greatly impairing quality of life and increasing healthcare expenditures.[2] Promoting healthy ageing by investigating the mechanisms of ageing and longevity is vital for society as a whole. The worldwide population of centenarians has also increased. Ageing affects all the cells and organs in the body, progressively resulting in functional impairment and loss of homoeostasis.[1] Specifically, ageing leads to profound alterations of the immune system, also called immunosenescence, which is defined as the dysfunction, destruction, and remodelling of the immune structure that occurs with ageing, resulting in poor vaccine outcomes, increased susceptibility to infection, and an increased incidence of age-related diseases and tumours.[3] A more recent study also demonstrated systemic chronic low-grade inflammation in older adults, known as "inflammageing".[4] More importantly, immunosenescence contributes to increased morbidity and mortality in older individuals by driving systemic and solid organs ageing.[5] Several studies have shown that natural killer (NK) cells, macrophages, T cells, and B cells experience minor to significant changes during immunosenescence.[4] For instance, the $CD8^+$ cytotoxic subset is sharply decreased in older individuals,[6] while age-associated B cells (ABCs) are upregulated in both aged mice and older adult humans.[7] Additionally, decreased numbers of $CD56^{bright}$ NK cells and increased numbers of $CD56^{dim}$ NK cells have been observed in ageing subjects.[8]

In contrast, centenarians are regarded as models of healthy ageing and exhibit different immune signatures than conventionally ageing subjects.[9] Therefore, in-depth study of centenarians could help uncover ageing-related changes in immune function and their underlying mechanisms, providing novel insights in coping with immunosenescence. Recent studies have used single-cell RNA sequencing (scRNA-seq) to investigate centenarians' immune structure and function. In 2019, Hashimoto et al. reported a marked increase in the number of cytotoxic $CD4^+$ T lymphocytes (CTLs) as a signature of Japanese supercentenarians.[10] Dong et al. reported that centenarians from Rugao city of China show an accumulation of granzyme B $(GZMB)^+$ and COX assembly mitochondrial protein homologue $(CMC1)^+$ CD8 T cells, with a naïve phenotype that transitions to a cytotoxic phenotype.[11] Karagiannis et al. demonstrated significant shifts in the ratios of lymphocytes to myeloid cells, noncytotoxic to cytotoxic cells, and $CD4^+$ T cells to B cells in centenarians from the United States.[12] However, these studies lacked comprehensive multi-omics integration and validation across diverse cohorts.

In this study, we used a droplet-based scRNA-seq platform (10× Genomics) to profile peripheral blood mononuclear cells (PBMCs) from centenarians (CENs), their offsprings (COs) and the offsprings' spouses or neighbours (controls, CTs) from Lingao County, Hainan Province in China, a well-known longevity island of the world. Moreover, scRNA-seq data of CENs and their controls from Rugao City and Japan were

downloaded from public databases with download link presented in previously published articles. A comprehensive analysis of the data from these three centenarian cohorts was conducted with the aim of identifying immune signature changes and increasing our understanding of the immune landscape of this population. Additionally, mass cytometry by time-of-flight (CyTOF) and flow cytometry were performed to further validate the scRNA-seq results and to provide more information about centenarians' immune signatures. Our findings are expected to shed light on the highly functional immune systems of centenarians, and provide experimental evidence to combat immunosenescence.

Methods

Participants and samples

The aim of this study was to explore the immune system characteristics related to longevity and healthy ageing. Individuals from three centenarian cohorts were enrolled. Healthy centenarians, offsprings with whom they live, and controls were screened as part of the Lingao centenarian cohort from the Hainan Province of China. Blood samples and clinical data were collected from all enrolled subjects. Their medical histories, including disorders of main organs/systems, infectious diseases, existing chronic diseases, and immune deficiency disorders, as well as histories of fractures and surgeries were investigated. The blood samples were sent to the clinical laboratory department to undergo blood routine examination, biochemistry analysis, immune function analysis, and infectious disease testing to rule out the presence of major acute or chronic infections, tumours, and major life-threatening diseases. Ultimately, 17 CENs, 9 COs, and 14 CTs were enrolled from the Lingao centenarian cohort, all of whom provided an informed consent form signed by themselves or their legal representatives.

Basic information regarding enrolled subjects and scRNA-seq/T cell receptor (TCR) data from seven CENs, six COs, and nine CTs in the Rugao centenarian cohort.[11] The basic information of enrolled samples and scRNA-seq data were downloaded from the Genome Sequence Archive for Human (https://ngdc.cncb.ac.cn/gsa-human/) under the accession number HRA002867. Another dataset from the Japanese centenarian cohort includes seven CENs, two COs, and three CTs.[10] The scRNA-seq data were downloaded from http://gerg.gsc.riken.jp/SC2018/.

Peripheral blood mononuclear cell isolation

Whole blood samples from the recruited subjects were mixed with an equal volume of Hank's balanced salt solution (HBSS, J67723.AP, Gibco, ThermoFisher Scientific, Waltham, MA, USA), then mixed with Ficoll–Paque PLUS (17-1440-02, GE Healthcare, Shanghai, China). The procedures were performed according to the manufacturer's instructions. The isolated PBMCs were later used for scRNA-seq, TCR-seq, CyTOF, and flow cytometry analyses.

Single-cell RNA sequencing and immune repertoire analysis

Single-cell RNA-seq and TCR libraries of the PBMCs from Lingao centenarian cohort using a Chromium platform (10× Genomics) and a Chromium Next GEM Single Cell 5′ Kit v2. Isolated PBMCs were washed with RPMI-1640 three times and concentrated to 600–1000 cells/μL, then immediately loaded onto a 10× microfluidic chip (10× Genomics) following the manufacturer's protocol to generate a complementary deoxyribonucleic acid (cDNA) library. Amplified cDNA was then used for both 50 gene expression library construction and TCR V(D)J targeted enrichment, which was performed with a Chromium Single Cell V(D)J Enrichment Kit and human T cell (10× Genomics), followed by V(D)J library construction. The raw sequencing data were aligned to the GRH38 reference genome using the *cellranger* (10× Genomics, V4.0, https://www.10xgenomics.com/cn) count and *vdj* functions.

To remove low-quality data and possible doublets, cells were excluded from the analysis if they fulfilled the following criteria: (1) gene numbers less than 400 or more than 6000; (2) unique molecular identifier (UMI) counts less than 1000 or more than 50,000; (3) percentage of mitochondrial RNA UMIs more than 10%; (4) number of genes per UMI (*log10GenesPerUMI*) less than 0.8. Ambient RNA was estimated using *DecontX* R package,[13] and cells with *decontX_contamination* values larger than 0.75 were excluded from further analysis. Also, cells with a high level of expression of more than one cell population-specific markers were removed. Red blood cells and platelets were discarded based on the expression of specific gene markers. Then, the gene expression count matrices of the three datasets were merged. Genes with low expression levels, defined as being expressed in no more than 100 cells, were excluded. Filtered count matrices were normalised using the *Normalise Data* function in *Seurat* (V4.3.0) and included in further analyses.[14]

Data integration and major PBMC population clustering

The top 2000 highly variable genes (HVGs) were detected using *FindVariableFeatures* [a function from Seurat (V4.3.0) R package] with default parameters. Two sources of unwanted variation—the total number of counts and the percentage of counts belonging to mitochondrial genes—were regressed using a linear model. Batch integration was performed during subsequent steps using the Seurat reciprocal principal-component analysis (*rPCA*) approach because of its

better performance in terms of batch-effect evaluation and correction.[14] Uniform manifold and approximation projection (UMAP) dimensional reduction and shared nearest neighbour graphs were generated using 30 principal components [the default number, as referenced by the official Seurat website, https://satijalab.org/seurat/articles/integration_rpca.html, accessed on Jan 5th, 2025]. Graph-based clustering was performed on the reduced data using a low resolution of 0.3 to effectively distinguish approximately 10 major cell types from each other.[15] Canonical marker genes were used to annotate the major cell populations. These genes were plotted on a dot plot to check the cell annotation.

PBMC sub-population–level analysis

After annotating the major PBMC populations, five major cell populations were re-clustered into sub-populations: $CD8^+$ T cells, $CD4^+$ T cells, γδ T (gdT) and NK cells, myeloid cells, and B cells. Sub-population clustering was performed similar to major cell clustering, as described above. The top 1500 HVGs were detected and used for further analysis. Then, the *rPCA* algorithm [a function from Seurat (V4.3.0) R package] was used to integrated the batch data, with the exception of B cells. While integrating B cells, *rPCA* function showed low performance, so we used *Harmony* R package for integration of this cell culster.[16] UMAP dimensional reduction and shared nearest neighbour graphs were generated using *rPCA*- or *Harmony*-corrected PCA embeddings. The resolution parameter for graph-based clustering was chosen individually for each sub-cluster. The number of clusters was selected based on matching clusters from reference datasets or clusters with specific highly expressed genes.[17] Specific highly expressed genes for each cell clusters were identified using the *FindMarker* function [a function from Seurat (V4.3.0) R package] with pct.1 larger than 0.5 and 1.5 times greater than pct.2 (pct.1 is the percentage of cells in the cluster where the gene is detected, while pct.2 is the percentage of cells on average in all the other clusters where the gene is detected). These cutoff values were set to obtain more specific marker genes.[15]

Differential gene expression analysis

Because the median value of *nFeature_RNA* (number of genes expressed per cell) was quite lower in the Japanese dataset than in the other two datasets, we did not include this dataset in the subsequent differentially expressed gene (DEG) analysis. Differential expression analysis between clusters was performed using a two-sided Wilcoxon rank-sum test with the *FindMarkers* function from the *Seurat* R package. The following parameters were used to filter DEGs: minimal percentage of cells per cluster expressing the gene equals 0.1, gene expression log 2 (fold change) threshold equals 0.2, and false discovery rate (FDR) adjusted P-value <0.05.[18] Genes that were up- or down-regulated in the Lingao and Rugao datasets were regarded as DEGs.

Single-cell TCR clonotype analysis

For the Lingao centenarian cohort, the Cell Ranger vdj pipeline V7.0.0 (available at 10× Genomics website) was used to perform reads alignment to the reference genome GRCh38 (GENCODE v32/Ensembl 98) and to assemble TCRs. Clonotype analysis of TCR was conducted using the *scRepertoire* toolkit based on the TCR-seq libraries. Each unique TCR α-chain(s)–TCR β-chain (s) pair was defined as a TCR clonotype. If one clonotype was present in at least two cells, the cells possessing this clonotype were regarded as clonal. Using the *clonalDiversity* function [a function from scRepertoire (V2.4.0) R package], the diversity across cell clusters was measured by the Shannon index. Using the *clonalOverlap* function [a function from scRepertoire (V2.4.0) R package], the clonotype overlap among cell clusters was then calculated and visualised using *Morisita* indexing. The *quantContig* function [a function from scRepertoire (V2.4.0) R package] was used to scale unique clonotypes to the size of the sample library.

Cell differentiation trajectory inference

Single-cell trajectories and pseudotime were calculated using *slingshot* (V2.6.0) R package with default parameters for $CD4^+$ T cells, $CD8^+$ T cells, and NK cells, separately.[19] Naïve cells were used as the starting point for the pseudotime analyses.

Gene set enrichment analysis

Enrichment analysis was performed using the *fgsea* R package.[20] Immune gene set collections were downloaded from the *ImmPort* database (https://www.immport.org/shared/home). As input for the enrichment analysis, genes were ranked based on average $\log_2$ (fold change) values, calculated using the *FindMarkers* function from the *Seurat* package.

Cell–cell communication analysis

To study interactions between cells and identify the mechanisms by which they communicate at single-cell resolution, the R package CellChat (V1.1.3) was applied, using default parameters.[21] Three types of interactions in the *CellChatDB* database were used: secreted signalling, cell–cell contact, and extracellular matrix (ECM)–receptor interactions. The calculated value "count" was used to indicate the interaction strength between pairs of cell clusters. The *computeCommunProb* function [a function from *CellChat* (V1.1.3) R package] was used to calculate the interaction weight between ligand–receptor pairs. *Cellchat* analysis of CEN and non-CEN sample groups was performed independently, and then the two groups were compared. Only the Lingao dataset was used for the cell–cell communication analysis. To more clearly study the interactions of NK

cells with other cells, we divided NK cells into two groups: neural cell adhesion molecule 1 (NCAM1, CD56) high-expressing and low-expressing subsets.

Transcription factor regulon activity

Single-cell–level regulon analysis was carried out using the *SCENIC* (single-cell regulatory network inference and clustering) R package in Python (*pySCENIC*).[22] The three datasets were analysed independently, and then common transcription factors (TFs) with high regulation scores in each dataset were selected as cell type–specific TFs and visualised using heatmap or UMAP plots. The regulatory network between TFs and their targets was visualised in *Cytoscape* (V3.6).

CyTOF sample processing

After isolating PBMCs using Ficoll, the cell precipitates were resuspended in 5 mL of pre-cooled fluorescence activated cell sorting (FACS) buffer [1× phosphate buffered saline (PBS) supplemented with 0.5% bovine serum albumin] and centrifuged at 400×*g* for 5 min at 4 °C. The supernatant was discarded and the cell precipitates were resuspended in FACS buffer. The number of cells was counted, and the quality of samples for subsequent analysis was assessed by the following criteria: the number of cells should not be less than 3×10^6, and the viability rate should be higher than 80%.

CyTOF staining and data acquisition

The provider, clone number, and mass tag of each antibody used in this study are shown in Supplementary Table S1. Antibody labelling with mass tags was performed using a Maxpar antibody conjugation kit (Fluidigm, San Francisco, CA, USA). The concentration of the mass-tagged antibody was assessed by NanoDrop (NanoDrop Technologies, Wilmington, DE). Antibody stabiliser buffer was used to adjust the concentration of the labelled antibody to 200 mg/mL. The obtained cells were washed with PBS, stained with 100 μL of 250 nmol/L cisplatin (Fluidigm) for 5 min on ice to exclude dead cells, and incubated in Fc receptor blocking solution before being stained with a surface antibody cocktail for 30 min on ice. After being washed with PBS, a unique barcoding isotope mixture was used to label individual cell samples for 30 min. The cells were washed twice with FACS buffer and fixed overnight in 200 μL of intercalation solution (Fluidigm). After fixation, the cells were washed with FACS buffer and then with Perm Buffer (00-4222, eBioscience, San Diego, CA, USA) and stained with an intracellular antibody cocktail for 30 min on ice. The cells were washed and resuspended in deionised water, mixed with 20% EQ™ beads (Fluidigm), and assessed on a mass cytometer (Helios, Fluidigm). The CyTOF experiments were performed by PLTTECH Inc. (Hangzhou, China). All samples were standardised to avoid batch effects before analysis.

CyTOF data analysis

The data for each sample were de-barcoded from the raw data using a doublet-filtering scheme with unique mass-tagged barcodes. Each .fcs file generated from different batches was normalised using the bead normalisation method.[23] We used *FlowJo* software (FlowJo, Ashland, Oregon, USA) to exclude debris, dead cells, and doublets from the manual gating data, leaving only live, single immune cells. The X-shift clustering algorithm was used to partition the cells into distinct phenotypes based on marker expression levels and then annotate the cell type of each cluster according to its marker expression pattern on a heatmap of clusters and markers.[24] A dimensionality reduction algorithm and t-distributed stochastic neighbour embedding were used to visualise the high-dimensional data in two dimensions to show the distribution of each cluster and marker expression, and the differences among the groups or different sample types.[25]

Flow cytometry analysis

The expression patterns of surface markers and transcriptional factors were determined by flow cytometry. The antibodies used for cell staining and subsequent flow cytometric analysis are listed in Supplementary Table S2. All of the flow cytometry experiments were carried out on a Beckman–Coulter DxFlex cell analyser (Miami, FL, USA), and the data were analysed with *FlowJo* software (V10.8.1). Briefly, to detect surface markers, PBMCs were isolated as described above, then washed twice with PBS containing 2% foetal bovine serum (FBS, A5256701, ThermoFisher, CA, USA) and stained for 30 min at 4 °C with labelled antibodies according to the manufacturers' recommendations.

For intracellular granzyme B and perforin staining, PBMCs were stimulated with Cell Stimulation Cocktail containing the protein transport inhibitor Brefeldin A (423303, Biolegend, San Diego, CA, USA) for 4 h. Then, the cells were stained for surface markers, fixed and permeabilised using a fixation/permeabilisation solution kit (554714, BD Biosciences, Franklin Lakes, NJ, USA). To detect the transcriptional factor runt-related transcription factor 3 (RUNX3), PBMCs were stained with surface marker-specific antibodies, permeabilised with reagents from the Foxp3/Transcription Factor Staining Buffer Set Kit (00-5523-00, eBioscience), and then stained with the relevant primary antibodies or isotype-matched control antibodies.

Statistical analysis

The statistical details for each experiment can be found in the respective figure legends. Data are presented as medians plus interquartile ranges. For comparisons of cell type–specific percentages, slingPseudotime, expression levels, and flow cytometry data across the CEN, CO, and CT groups, post-hoc Dunn's test was used after a one-way Kruskal–Wallis test with

Bonferroni adjustment. Statistical analyses were performed using R software (V4.1.2) and GraphPad Prism (V10.4.1). The sample size, name, and type of statistical test are stated in each figure legend. All applied tests were nonparametric, and thus no assumptions were made regarding the normality of the data distribution.

Ethics

This study was approved by the Ethics Committee of Hainan Hospital of the Chinese PLA General Hospital (No. S2023-287). All participants provided written informed consent prior to their enrolment.

Role of funders

The funding sources did not play any role regarding the study's design, data acquisition, data analysis, results interpretation, or report writing.

Results

Cellular profiling of peripheral immune cells using scRNA-seq analysis

To better understand the comprehensive immune remodelling that occurs in centenarians, we conducted scRNA-seq analyses of the immune cell populations of PBMCs collected from 19 CENs, 10 COs, and 15 CTs from three centenarian cohorts (scRNA-seq data from Rugao and Japanese cohorts were downloaded from public databases provided in previously published articles) (Fig. 1A and B). The detailed information of the individuals from Lingao and Rugao centenarian cohorts, including previous medical history, body mass index (BMI), chronic diseases, immune deficiency disorders, main laboratory tests (routine blood test, blood biochemistry test, tumour biomarker test, and serological testing for infectious diseases) are presented in Supplementary Table S3. The CENs and their controls were all in good health, without major infections, tumours, or life-threating diseases. After rigorous data quality control and filtering, a total of 229,929 cells were acquired, with age, sex, median gene counts and UMI counts provided (Fig. 1C, Supplementary Table S4). The UMAP plot in Fig. 1C shows 10 major cell clusters identified by the expression patterns of known lineage markers and the top five differentially expressed genes (DEGs). The PBMC cell populations from the three CEN cohorts are presented with UMAP plots showing cell cluster and density distributions (Supplementary Fig. S1A, B). In detail, the major cell clusters that were identified included 70,448 $CD4^+$ T cells (*CD3D*, *CD4*), 45,413 $CD8^+$ T cells (*CD3D*, *CD8B*), 10,671 gdT cells [*CD3*, T cell receptor delta constant (*TRDC*), T cell receptor gamma constant (*TRGC*)], 3582 mucosal-associated invariant T cells (MAITs) [killer cell lectin-like receptor B1 (*KLRB1*), solute carrier family 4 member 10 (*SLC4A10*), dual specificity phosphatase 2 (*DUSP2*)], 47,441 NK cells [Fc gamma receptor IIIa (*FCGR3A*), natural killer cell granule protein 7 (*NKG7*), killer cell lectin like receptor D1 (*KLRD1*), granulysin (*GNLY*)], 13,426 B cells [*CD79A*, immunoglobulin kappa constant (*IGKC*), membrane spanning 4-domains A1 (*MS4A1*)], 4335 megakaryocytes (Meg) [pro-platelet basic protein (*PPBP*), platelet factor 4 (*PF4*), glycoprotein IX platelet (*GP9*)], 33,245 myeloid cells [lysozyme (*LYZ*), S100 calcium binding protein A8 (*S100A8*), S100 calcium binding protein A9 (*S100A9*)], 221 progenitor cells [*CD34*, GATA binding protein 2 (*GATA2*), SRY-box transcription factor 4 (*SOX4*)] and 1147 proliferative T/NK cells [marker of proliferation Ki-67 (*MKI67*), stathmin 1 (*STMN1*), DNA topoisomerase II alpha (*TOP2A*)] (Fig. 1C and D, Supplementary Fig. S1C). The densities and distributions of these 10 major cell clusters across the CEN, CO and CT groups are presented in Fig. 1E. There were striking differences in the percentages of $CD4^+$ T cell, $CD8^+$ T cell, and NK cells across CENs, COs, and CTs, with COs exhibiting an intermediate phenotype between CENs and CTs. A decrease in the frequencies of B cells ($P < 0.05$), $CD4^+$ T cells ($P < 0.001$), and MAIT cells ($P < 0.01$), with an increase in the frequency of NK cells ($P < 0.01$) and proliferative T/NK cells ($P < 0.01$) in the CEN group compared with the findings in the CTs (Fig. 1F and G). Compared with the COs, the CENs exhibited similar frequencies of the major cell clusters, with the exception of a significant decrease in MAIT cells ($P < 0.01$). These findings provide detailed information about the changes in immunological features of CENs compared with those of COs and CTs.

Unique patterns of cell cluster frequencies in centenarians associated with age and sex

To further investigate the changes in cell cluster that occur with age, the enrolled subjects were further divided into subgroups according to their ages. Because most of the COs and CTs from the three centenarian cohorts were older than 60, to better show the changes in cell percentages with age, scRNA-seq data of 12 healthy controls (aged from 30 to 58 years) from dataset GSE158055 were downloaded and incorporated into the age-associated analysis (Supplementary Fig. S2A, B).[26] The subjects were further classified into nine subgroups according to their ages. As shown in Supplementary Fig. S2C, the percentage of MAITs decreased as age increased ($P < 0.05$), while the percentages of gdT cells and proliferative T/NK cells increased as age increased ($P < 0.01$, $P < 0.05$, respectively). Interestingly, myeloid cells showed a unique pattern of first decreasing and then increasing as age increased ($P < 0.01$). The other major cell clusters did not exhibit significant trends as age increased.

The centenarians and controls were then divided according to their sex and age into four groups, namely CENF (female centenarians), CENM (male centenarians),

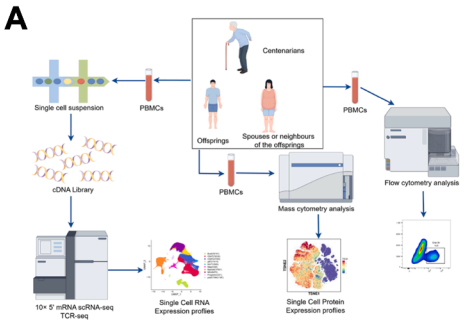

B

Cohort Name	Centenarians	Offsprings	Controls
Lingao Cohort	17	9	14
Sex	8 males, 9 females	9 males	3 males, 11 females
Age (Median)	103	62	60
Rugao Cohort	7	6	9
Sex	2 males, 5 females	2 males, 4 females	3 males, 6 females
Age (Median)	100	67.5	68
Japan Cohort	7	2	3
Sex	2 males, 5 females	1 male, 1 female	1 male, 2 females
Age (Ranges)	>110	70~80	60~80

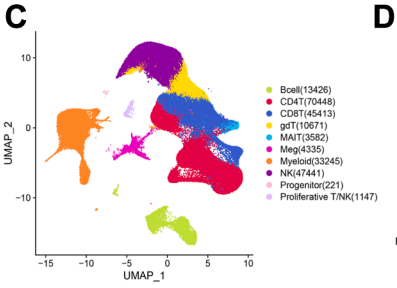

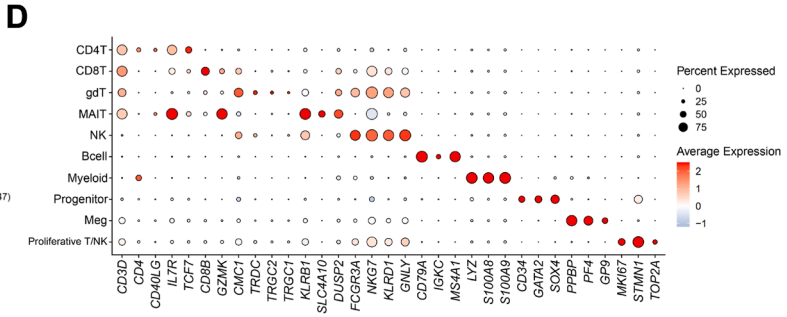

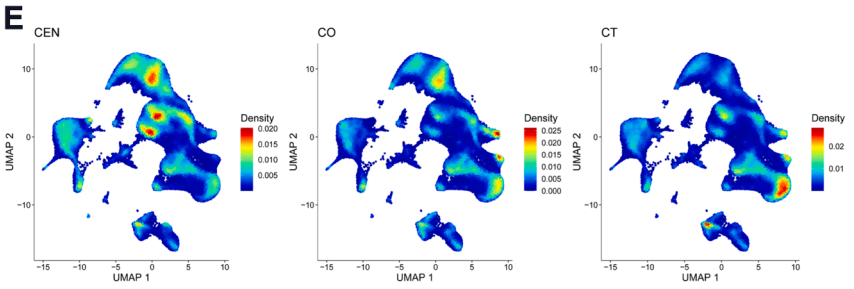

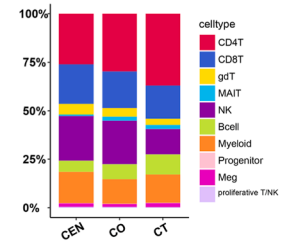

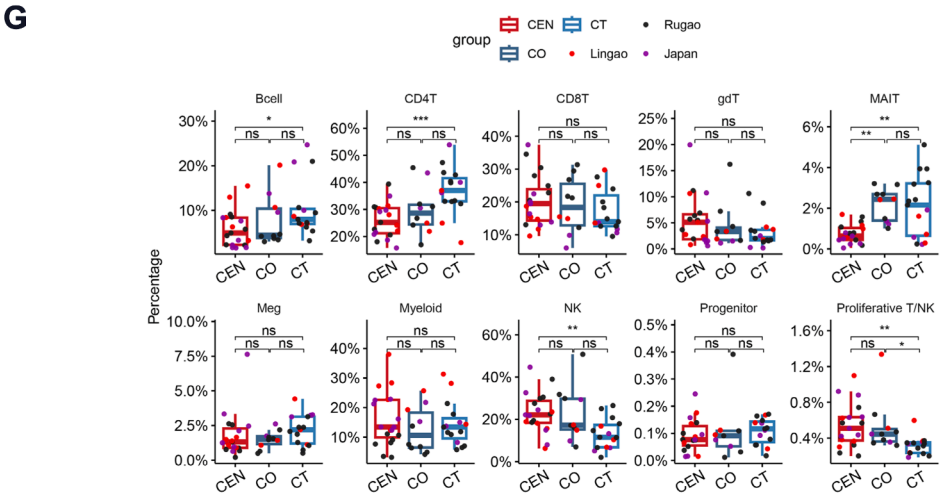

***Fig. 1:* Global analysis of immune cell populations in PBMCs from CENs and their younger controls**. (A, B) Project landscape of this study. PBMCs isolated from centenarians, their offsprings (COs) and the offsprings' spouses or neighbours (controls, CTs) were used for scRNA-seq, CyTOF and flow cytometry analyses. PBMCs from a total of 19 CENs, 10 COs and 15 CTs from three cohorts were enrolled for scRNA-seq analysis. The basic information of included subjects from three CEN cohorts was presented in (B). The scRNA-seq data of Rugao and

CO + CTF (female COs and CTs), and CO + CTM (male COs and CTs). Compared with the findings in the CO + CTs, an increased percentage of proliferative T/NK cells ($P < 0.01$) was seen in female CENs, but not in males. Compared with the findings in the CO + CTs, significantly decreased percentages of $CD4^+$ T cells ($P < 0.05$) and MAIT cells ($P < 0.01$) in CENs were seen in male CENs, but not in female CENs (Supplementary Fig. S3). These results indicate that sex may affect PBMCs composition in centenarians.

Cellular profiling of peripheral immune cells by CyTOF

To further investigate the immune profiles of centenarians and validate the scRNA-seq results, PBMCs from nine CENs, six COs, and five CTs from the Lingao centenarian cohort were analysed by mass cytometry. Using an antibody panel consisting of 42 antibodies (Supplementary Table S1), CyTOF data were preprocessed and living single immune cells ($CD45^+$) were retained after gating for further analysis. Eleven cell clusters from the enrolled subjects were identified on the constructed heatmap (Fig. 2A), and the t-distributed stochastic neighbour embedding (t-SNE) map shows the peripheral immune cells and all the cell surface markers used for annotation (Fig. 2B, Supplementary Fig. S4). The major cell clusters included $CD4^+$ T cells ($CD3^+CD4^+CD8^-$), $CD8^+$ T cells ($CD3^+CD4^-CD8^+$), B cells ($CD3^-CD19^+CD20^+$), conventional dendritic cells (DCs, $CD3^-CD19^-CD14^-$HLA-DR^+CD11b^+), monocytes ($CD3^-CD19^-CD14^+CD33^+$ HLA-DR^+), granulocytes ($CD3^-CD19^-CD14^-CD11^+$ $CD16^+$), myeloid-derived suppressor cells (MDSCs, $CD3^-CD19^-CD11^+$HLA-DR^-CD33^+), NK cells ($CD3^-$ $CD19^-CD14^-CD56^+$), NKT cells ($CD3^+CD19^-CD14^-$ $CD56^+$), γδ T cells ($CD3^+CD20^-$TCRgd$^+$), and plasmacytoid dendritic cells (pDCs, $CD3^-CD19^-CD14^-CD20^-$ HLA-DR^+CD123^+). Box plots showed a decreased percentage of B cells in CENs compared with that in COs ($P < 0.05$); the percentage of $CD4^+$ T cells was decreased in CENs compared with that in CTs ($P < 0.01$); and the percentage of NK cells was increased in CENs compared with that in CTs ($P < 0.05$) (Fig. 2C and D). These results are highly consistent with the cell proportions determined from the scRNA-seq data. Together with the scRNA-seq–based definition of cell clusters, these results further validate the peripheral immune cell atlas of CENs.

Changes in $CD4^+$ T cells in centenarians compared with those in their younger controls

We next performed a detailed analysis of $CD4^+$ T cells, identifying nine $CD4^+$ T cell subsets based on the expression patterns of functional genes: $CD4^+$CTL cells (CD4_CTL), interferon (IFN)$^+CD4^+$ T cells (CD4_IFN), $CD4^+CD27^+$ central memory T cells (Tcm) (CD4_Tcm_CD27), $CD4^+$Th1 cells (CD4_Th1), $CD4^+$Th2 cells (CD4_Th2), $CD4^+$Th17 cells (CD4_Th17), $CD4^+$Th22 cells (CD4_Th22), $CD4^+$ naïve T cells ($CD4^+$Tn, CD4_Tn), and $CD4^+$ regulatory T cells ($CD4^+$Tregs, CD4_Treg) (Fig. 3A and B). Density analysis of the UMAP plot showed that COs exhibit an intermediate phenotype between CENs and CTs (Fig. 3C), while similar cell distribution patterns were observed across the Lingao, Rugao, and Japan groups (Supplementary Fig. S5A). Box plots revealed that a dramatic increase in the percentage of the $CD4^+$CTL cells and decreased percentages of $CD27^+CD4^+$ Tcm, $CD4^+$Th17 and $CD4^+$Tn cells in CENs compared with those in CTs (Fig. 3C and D).

To further investigate the differentiation trajectories of the $CD4^+$ T cell subsets, a time series analysis was conducted. $CD4^+$Tn cells were located at the beginning of the timeline, while CTL cells, Tregs, and Th17 cells were at the pseudo-temporal endpoints, forming three differentiation branches. Significant differences were observed across the CEN, CO, and CT groups regarding the pseudotime values of the $CD4^+$ T cells. Although $CD4^+$ T cells from CENs were located at later pseudotime positions in all three trajectories, $CD4^+$ T cells from CENs were inclined to differentiate into $CD4^+$CTL cells (Fig. 3E–G). TCR-seq analysis demonstrated that $CD4^+$Tn cells exhibited the most abundant unique clonotypes, while $CD4^+$CTL cells were rich in hyperexpanded clonotypes (Supplementary Fig. S5B, C).

Because the median gene counts of subjects from the Japanese cohort were low, DEGs were identified using the data from the Rugao and Lingao cohorts. The volcano plot showed that, compared with control subjects, CENs exhibited upregulation of cytotoxic genes [*GNLY*, *GZMA* (granzyme A), *GZMH* (granzyme H)] and antigen processing/presentation genes (*HLA-DRB5*, *HLA-DRB1*) and downregulation of naïve-associated gene [Lymphoid enhancer-binding factor 1 (*LEF1*)] or inflammatory genes (*NFKBIA*, *NFKBIZ*) (Supplementary Fig. S5D). Gene set enrichment analysis (GSEA) demonstrated enhanced antigen

Japan cohorts were downloaded from public databases. (C) Uniform manifold and approximation projection (UMAP) plot of the identified cell clusters of PBMCs, coloured by the cell clusters. GdT, γδ T cells; MAIT, mucosal-associated invariant T cells; Meg, megakaryocytes; NK, natural killer cells. (D) Expression levels of top expressed DEGs per cell type. The size of the dot means proportion of cells with expression in each cluster, while colour of the dot means average expression in each cluster. (E) UMAP plots of all PBMC clusters with cell proportion density, dividing into CEN, CO and CT groups. (F) Proportional distribution of each major cell cluster in CEN, CO and CT groups. (G) Box plots showing the percentages of each major cell cluster in CEN, CO and CT groups by incorporating the scRNA-seq data of three cohorts. The percentages of cell clusters were presented as medians plus interquartile ranges. $N_{CEN} = 19$, $N_{CO} = 10$, and $N_{CT} = 15$. Statistical significance was determined using the Kruskal–Wallis test followed by Dunn's multiple comparison tests. (*$P < 0.05$, **$P < 0.01$, ***$P < 0.001$, ns, not significant).

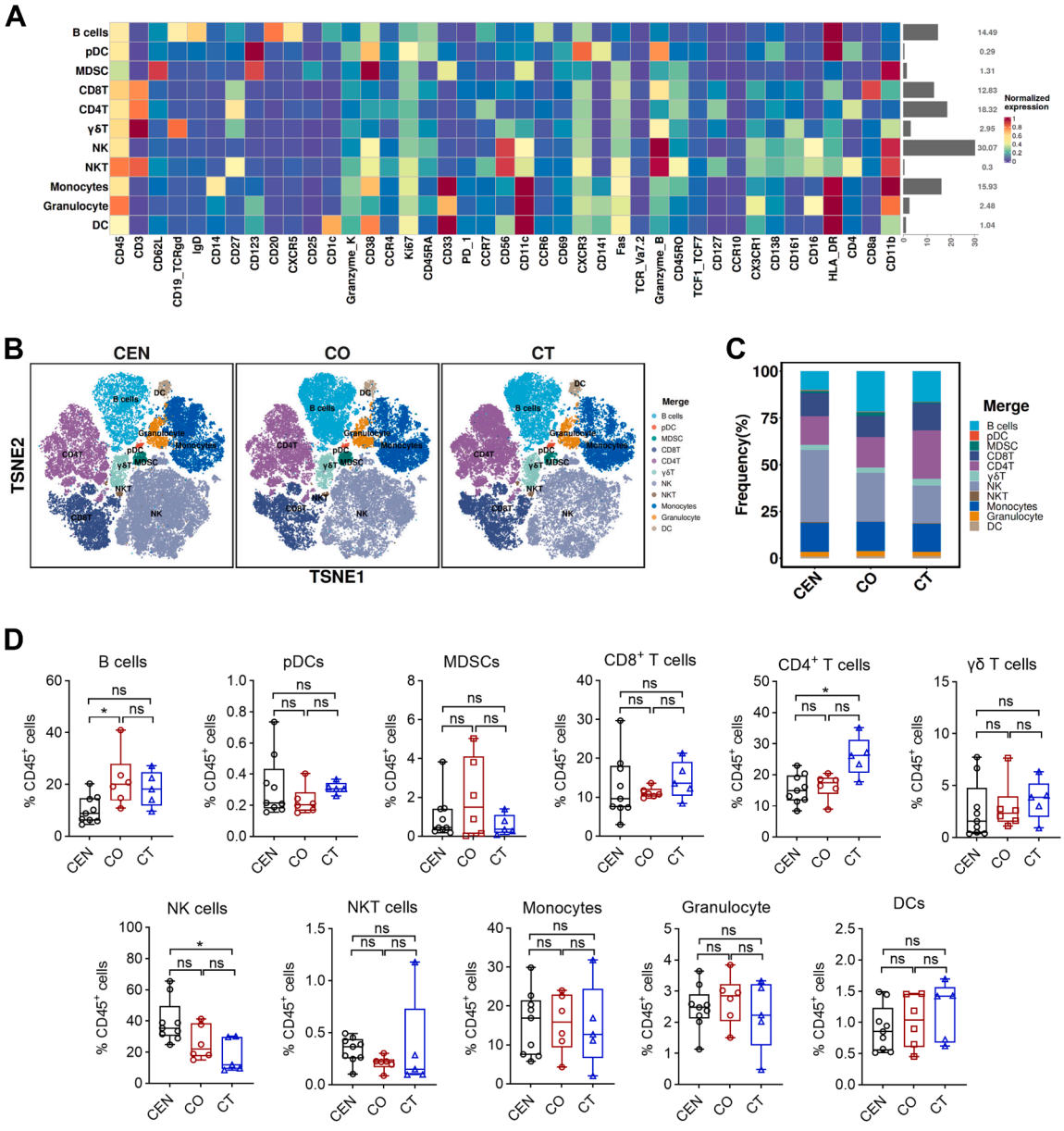

***Fig. 2:* Single-cell CyTOF analysis reveals the peripheral immune landscape of CENs and their younger controls.** (A) Heatmap displaying normalised median marker expressions of the identified eleven major cell clusters. The bar plot on the right represents the relative frequencies of cell clusters. The annotated cell types are labelled on the left correspondingly. (B) Visualised t-SNE showing the distributions of major cell clusters from CyTOF data, dividing into three groups (nine CENs, six COs, and five CTs). (C) Proportional distribution of each major cell cluster in CEN, CO and CT groups using CyTOF. (D) Box plots showing the percentages of each major cell type in CEN, CO and CT groups. The percentages of cell clusters were presented as medians plus interquartile ranges. N_{CEN} = 9, N_{CO} = 6, and N_{CT} = 5. Statistical significance was determined using the Kruskal–Wallis test followed by Dunn's multiple comparison tests. (*P < 0.05, ns, not significant).

processing and presentation, cell cytotoxicity, cytokine, and antimicrobial pathways in CENs compared with the findings in control subjects (Supplementary Fig. S5E, F).

T cell differentiation and function is largely coordinated by the activity of TFs. $CD4^+$T cells in the CEN group displayed significantly different regulon activities for certain TFs, such as RUNX3, LEF1 and nuclear factor of activated T-cells, cytoplasmic 2 (NFATC2) (Fig. 3H). Specifically, $CD4^+$T cells from CENs exhibited higher mRNA levels of *RUNX3* and *NFATC2* expression and lower levels of *LEF1* expression (Fig. 3I

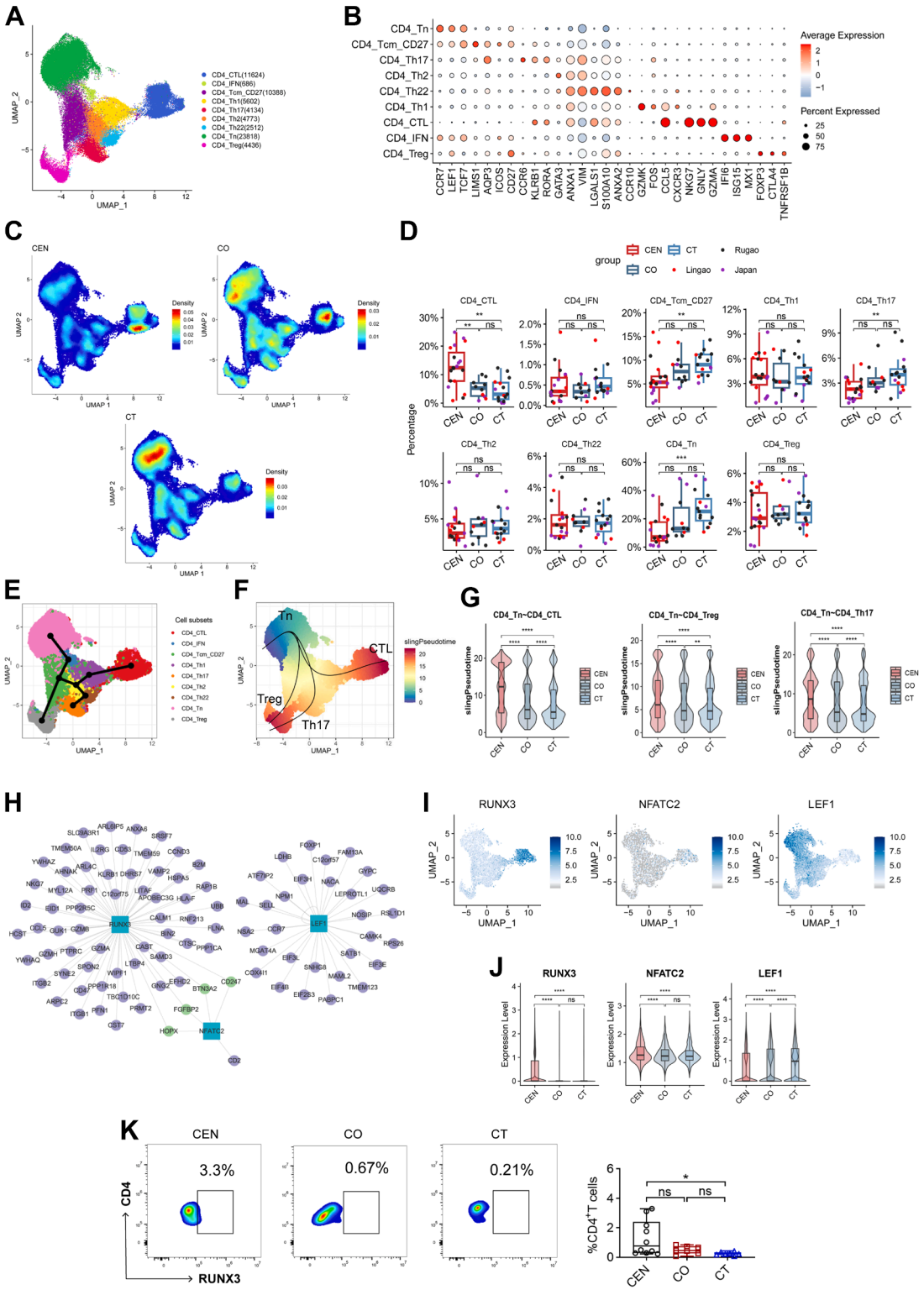

***Fig. 3:* Characterisation of CD4⁺ T cells phenotypes in centenarians compared with those in their younger controls.** (A) UMAP plot showing the clustering of CD4⁺ T cells, identifying 9 cell subsets. CD4_CTL, CD4⁺ CTL cells; CD4_IFN, IFN⁺CD4⁺ T cells; CD4_Tcm_CD27, CD4⁺CD27⁺Tcm cells; CD4_Th1, CD4⁺ Th1 cells; CD4_Th17, CD4⁺ Th17 cells; CD4_Th22, CD4⁺ Th22 cells; CD4_Tn, CD4⁺ naïve T cells;

and J). Flow cytometry analysis validated that RUNX3 expression was significantly upregulated in CD4$^+$T cells from CENs compared with that in those from CTs ($P < 0.05$), but not in those from COs (Fig. 3K, Supplementary Fig. S6). These TFs cooperatively drive CD4$^+$ T cells to upregulate cytotoxicity and downregulate the naïve phenotype.

Changes in CD8$^+$ T cells in centenarians compared with those in their younger controls

Next, we performed a detailed analysis of CD8$^+$ T cells, identifying six CD8$^+$ T cell subsets based on the expression of functional genes: CMC1$^+$CD8$^+$ T cells (CD8_CMC1), CD8$^+$CTL cells (CD8_CTL), HLA-DRs$^+$CD8$^+$ T cells (CD8_HLA-DRs), GZMK$^+$CD8$^+$Tcm cells (CD8_Tcm_GZMK), proteolipid protein 2 (PLP2)$^+$CD8$^+$Tcm cells (CD8_Tcm_PLP2), and CD8$^+$Tn cells (CD8_Tn) (Fig. 4A and B). Density analysis of the UMAP plots and cell proportion analysis of the box plots revealed a dramatic increase in the percentages of CD8$^+$CTL cells and CMC1$^+$CD8$^+$ T cells with decreased percentages of CD8$^+$Tn cells in CENs compared with the findings in CTs (Fig. 4C and D). CyTOF analysis further validated these changes, showing a decreased percentage of CD8$^+$Tn cells in CENs compared with the percentages in COs and CTs (Fig. 4E). These findings are consistent with a previous study.[11] Density analysis of the UMAP plots showed that the cell distributions were similar between the Lingao and Rugao cohorts, while the Japanese cohort exhibited a relatively different distribution pattern (Supplementary Fig. S7A). CD8$^+$CTL cells were located at the endpoint of the differentiation trajectory, while CMC1$^+$CD8$^+$ T cells were located at a transitional position. The other two trajectories developed into HLA-DRs$^+$CD8$^+$ T cells and PLP2$^+$CD8$^+$Tcm cells. Significant differences in pseudotime values were observed in all three trajectories: CD8$^+$T cells from CENs were more likely to differentiate into CD8$^+$CTL cells and HLA-DRs$^+$CD8$^+$ T cells than those from COs and CTs (Fig. 4F–H). TCR-seq analysis showed that CMC1$^+$CD8$^+$ T cells, GZMK$^+$CD8$^+$Tcm cells, and CD8$^+$Tn cells exhibit more unique clonotypes compared with other cell subsets, while CD8$^+$CTL cells exhibited the largest percentage of cells with hyperexpanded clonotypes (Supplementary Fig. S7B, C). The volcano plot indicated upregulation of cytotoxic genes (*GZMA*, *CMC1*) and antigen processing/presentation genes (*HLA-DPs*, *HLA-DRs*, and *HLA-DQs*), and downregulation of naïve T cell–associated genes [Interleukin-7 receptor (*IL7R*), L-selectin (*SELL*), *LEF1*] (Supplementary Fig. S7D). The violin plots demonstrated upregulated mRNA expressions of cytotoxic markers [*GZMA*, *GZMB*, *GZMH*, and *perforin 1* (*PRF1*)] and MHC molecules (*HLA-DRA* and *HLA-DQA1*) in CD8$^+$ T cells from CENs compared with those from their younger controls (Fig. 4I). GSEA also revealed enhanced chemokine and cytokine productions, antigen processing and presentation, TCR signalling, and antimicrobial functions (Supplementary Fig. S7E). These results suggest that CD8$^+$ T cells in CENs exhibited enhanced cytotoxic functions and antigen presentation capacities that maintain immune function.

Changes in B cells in centenarians compared with those in their younger controls

Detailed analysis of B cells identified eight B cell subsets based on the expression of functional genes: ABC cells, naïve B cells, IFN$^+$ naïve B cells (Naïve B_IFN), non-switched memory B cells, plasma B cells, proliferative B cells, switched memory B cells, and transitional B cells (Supplementary Fig. S8A, B). Density analysis of the UMAP plots and cell proportion analysis of the box plots revealed only small changes in the percentages of B cell subsets, with decreased percentage of non-switched memory B cells in CENs compared with the percentages of those in COs or CTs (Supplementary Fig. S8C, D). TF analysis revealed that JUNB is at the centre of B cell development, with upregulated expression levels of *JUNB*, *FOS*, *POU2F2* (POU domain, class 2, transcription factor 2), and *JUND* compared with the findings in COs and CTs (Supplementary Fig. S8E–G).

Changes in myeloid cells in centenarians compared with those in their younger controls

Eleven myeloid cell subsets were identified based on the expression of functional genes: CD14$^+$ monocytes (CD14mono), CD14$^+$HLA^{high} monocytes (CD14mono_HLA.h), CD14$^+$IFN$^+$ monocytes (CD14mono_IFN), CD14$^+$IL1B$^+$ monocytes (CD14mono_IL1B), CD14$^+$MALAT1^{high} monocytes (CD14mono_MALAT1.h), CD16$^+$ monocytes (CD16mono), CD16$^+$HLA^{high}

CD4_Treg, CD4$^+$ regulatory T cells. (B) Expression of top expressed marker genes per cell subset. (C) UMAP plots of CD4$^+$ T cells with cell proportion density, dividing into CEN, CO and CT groups. (D) Box plots showing the percentages of key subsets of CD4$^+$ T cells in CEN, CO, and CT groups by incorporating the scRNA-seq data of three cohorts. The percentages of cell subsets were presented as medians plus interquartile ranges. $N_{CEN} = 19$, $N_{CO} = 10$, and $N_{CT} = 15$. (E, F and G) UMAPs showing the differentiation trajectory of CD4$^+$ T cell subsets, with the difference of pseudotime analyses across CEN, CO and CT groups. $N_{CEN} = 19$, $N_{CO} = 10$, and $N_{CT} = 15$. (H, I and J) Key TFs network analysis, with the expression patterns and distribution analyses of these TFs in UMAPs. $N_{CEN} = 19$, $N_{CO} = 10$, and $N_{CT} = 15$. (K) Representative flow cytometry plots of RUNX3–expressing CD4$^+$ T cells (left). Comparison of the frequency of RUNX3–expressing cells in CD4$^+$ T cells across CEN, CO and CT groups (right). The percentages of cell subsets were presented as medians plus interquartile ranges. $N_{CEN} = 10$, $N_{CO} = 7$, and $N_{CT} = 7$. All the statistical significance was determined using the Kruskal–Wallis test followed by Dunn's multiple comparison tests. (*$P < 0.05$, **$P < 0.01$, ***$P < 0.001$, ****$P < 0.0001$, ns, not significant).

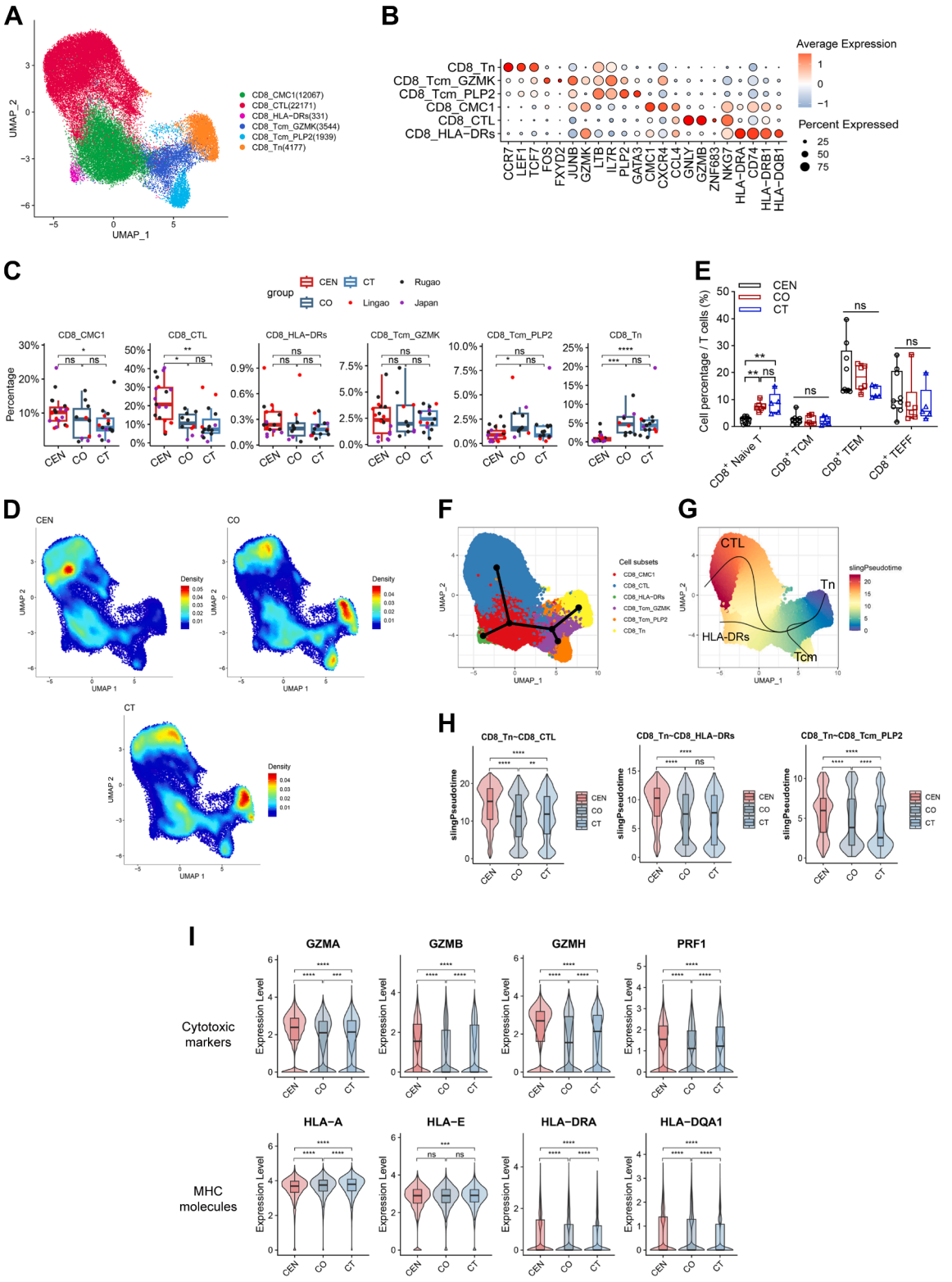

Fig. 4: **Characterisation of CD8⁺ T cells phenotypes in centenarians compared with those in their younger controls**. (A) UMAP plot showing the clustering of CD8⁺ T cells, identifying six cell subsets. CD8_CMC1, CMC1⁺CD8⁺ T cells; CD8_CTL, CD8⁺ CTL cells; CD8_HLA-DRs,

monocytes (CD16mono_HLA.h), macrophage, myeloid DCs (mDC), neutrophils, and plasmacytoid DCs (pDC) (Supplementary Fig. S9A, B). Density analysis of the UMAP plots and cell proportion analysis of the box plots revealed only small changes in myeloid cell subsets, with a decreased percentage of mDCs in CENs compared with that in COs (Supplementary Fig. S9C, D). GSEA demonstrated enhanced cytokine and chemokine productions, and antimicrobial functions in myeloid cells from CENs compared with the findings in COs and CTs (Supplementary Fig. S9E). Therefore, small changes in cell subset percentages and enhanced immune functions were the main signatures of myeloid cells in CENs.

Changes in NK and γδ T cells in centenarians compared with those in their younger controls

NK cells were further classified into four subsets: high affinity immunoglobulin epsilon receptor subunit gamma (*FCER1G*)$^{+}$NK cells (NK_FCER1G), IFN^{+}NK cells (NK_IFN), IL32^{high}NK cells (NK_IL32.h), and NCAM1^{high}NK cells (NK_NCAM1.h). γδ T cells were further classified into three subsets according to the expression of functional genes: IL7R^{+} gdT cells (gdT_IL7R), TRGC^{+} gdT cells (gdT_TRGC), and TRGV^{+} gdT cells (gdT_TRGV) (Fig. 5A and B). Density analysis of the UMAP plots and cell proportion analysis of the box plots revealed only small changes in the percentages of NK cell subsets, with a decreased percentage of NCAM1^{high} NK cells in CENs compared with that in CTs (Fig. 5C and D). The percentage of naïve gdT cells (IL7R^{+}) was significantly decreased in CENs compared with the percentages in COs and CTs, and an increased percentage of TRGC^{+} gdT cells was observed in CENs compared with the percentages in COs and CTs (Fig. 5C and D). Density analysis of the UMAP plots from the Lingao, Rugao, and Japan cohorts revealed that the cell subset distribution patterns were similar between the Lingao and Rugao cohorts (Supplementary Fig. S10A). CyTOF analysis was performed to further investigate the proportions of NK cell subsets. NK cells were further classified as CD56^{dim}CD16^{+} or CD56^{bright}CD16^{-}. There was no significant difference in the percentage of these two NK cell subsets across CENs, COs, and CTs (Fig. 5E).

Next, the mRNA expression levels of key TFs in NK cells were assessed. *RUNX3* and *Krüppel-like factor 4* (*KLF4*) were upregulated, *FOS* was downregulated, and *FOSB* exhibited no change in expression levels in CENs compared with the findings in CTs (Fig. 5F–H). Additionally, RUNX3 and KLF4 regulon activities were significantly upregulated in all three cohorts (Supplementary Fig. S10B). Flow cytometry analysis further validated that RUNX3 expression levels were significantly upregulated in CD56^{dim} NK cells from CENs compared with the levels in those from CTs ($P < 0.001$), but not in those from COs (Fig. 5I, Supplementary Fig. S6).

NK cells exhibited only one differentiation trajectory, with NCAM1^{high}NK cells located at the beginning of the timeline trajectory and IL32^{high}NK cells located at the pseudo-temporal endpoint. NK cells from CENs located at earlier pseudotime positions in the trajectory compared with those from COs and CTs (Supplementary Fig. S10C–E), indicating relatively "young" signatures. GSEA analyses of NK cells indicated that antimicrobial function and cytokine receptor signalling were upregulated, while antigen processing/presentation was downregulated, in CENs compared with the findings in CO plus CT subjects (Supplementary Fig. S10F). Most gdT cell immune functions were enhanced in CENs compared with those in CO plus CT subjects (Supplementary Fig. S10G). The above results indicated that NK cells exhibited similar subset abundance and enhanced immune function in CENs compared with those in control subjects.

Enhanced cell cytotoxicity and discrepant membrane receptor expression patterns in NK cells from centenarians compared with their younger controls

To better investigate the functional status of NK cells in CENs, we further analysed the expression patterns of cytotoxic genes in NK cells. scRNA-seq data analysis showed, although with statistical significance, the fold changes in *GZMA*, *GZMB*, *GZMH*, and *PRF1* mRNA expression levels did not change greatly across CENs, COs and CTs (Fig. 6A). Next, isolated PBMCs were treated with a cell stimulation cocktail, and NK cells were gated for detailed analyses of cytotoxic proteins.

HLA-DRs^{+}CD8^{+} T cells; CD8_Tcm_GZMK, CD8^{+}GZMK^{+}Tcm cells; CD8_Tcm_PLP2, CD8^{+}PLP2^{+}Tcm cells; CD8_Tn, CD8^{+} naïve T cells. (B) Expression of top expressed marker genes per cell subset. (C) Box plots showing the percentages of key CD8^{+} T cell subsets in CEN, CO, and CT groups by incorporating the scRNA-seq data of three cohorts. The percentages of cell subsets were presented as medians plus interquartile ranges. $N_{CEN} = 19$, $N_{CO} = 10$, and $N_{CT} = 15$. (D) UMAP plots of CD8^{+} T cells with cell proportion density, dividing into CEN, CO and CT groups. (E) CyTOF analysis revealed the percentages of key CD8^{+} T cell subsets [CD8^{+} naïve T cells, CD8^{+} TCM, CD8^{+} effector memory T (TEM) cells, effector CD8^{+} T cells (CD8^{+} TEFF)] in CEN, CO and CT groups. The percentages of cell subsets were presented as medians plus interquartile ranges. $N_{CEN} = 9$, $N_{CO} = 6$, and $N_{CT} = 5$. (F, G and H) UMAP plots showing the differentiation trajectories of CD8^{+} T cell subsets, with the comparisons of pseudotime values across CEN, CO and CT groups. $N_{CEN} = 19$, $N_{CO} = 10$, and $N_{CT} = 15$. (I) The violin plots showing the expression difference of cytotoxic and MHC molecules. $N_{CEN} = 19$, $N_{CO} = 10$, and $N_{CT} = 15$. All the statistical significance was determined using the Kruskal–Wallis test followed by Dunn's multiple comparison tests. (*$P < 0.05$, **$P < 0.01$, ***$P < 0.001$, ****$P < 0.0001$, ns, not significant).

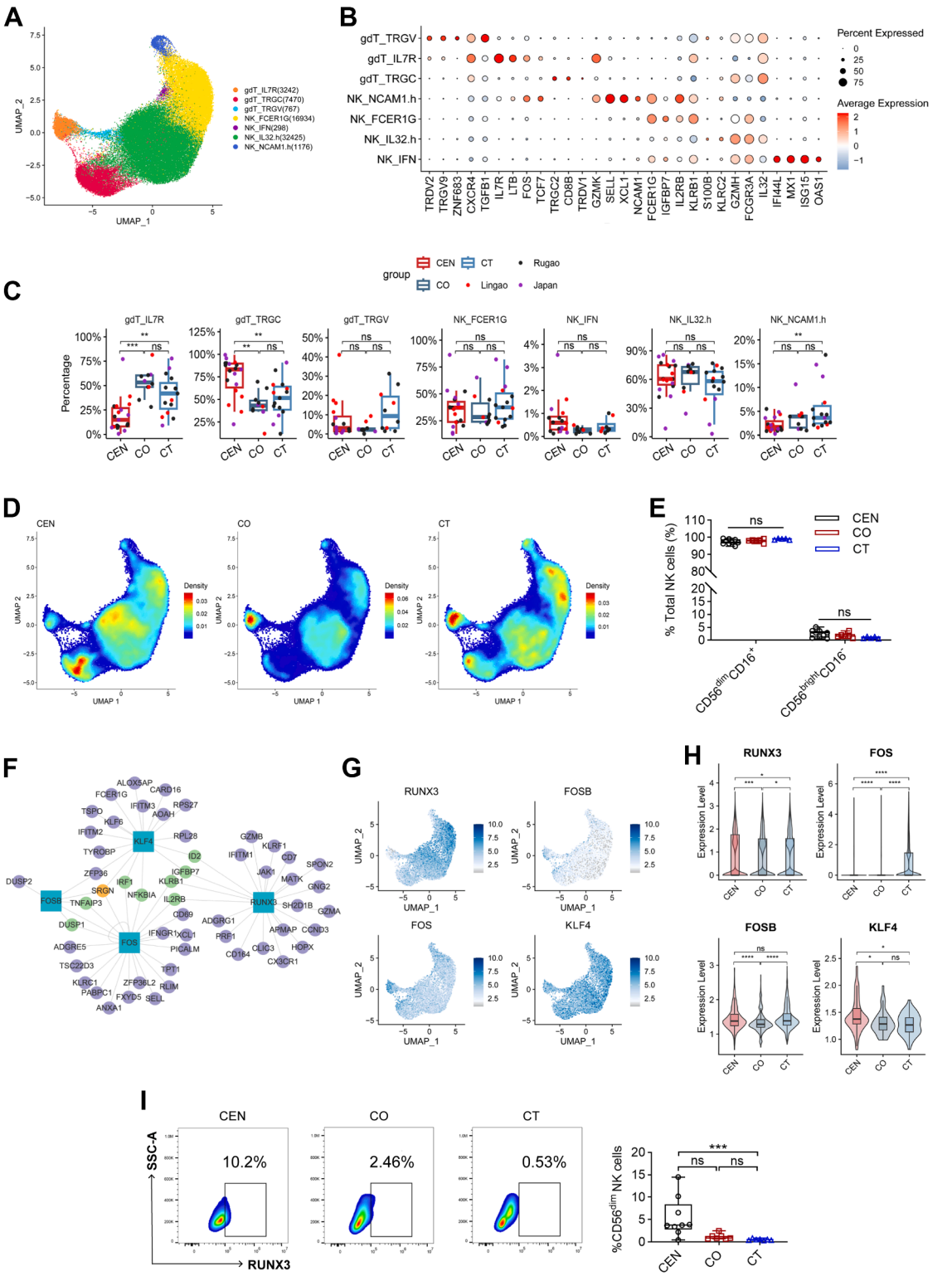

Fig. 5: **Characterisation of NK and γδ T cells phenotypes in centenarians compared with those in their younger controls.** (A) UMAP plot showing the clustering of NK and γδ T cells, identifying 7 cell subsets. GdT_IL7R, IL7R^{+}γδ T cells; gdT_TRGC, TRGC^{+}γδ T cells; gdT_TRGV, TRGV^{+}γδ T cells; NK_FCER1G, FCER1G^{+}NK cells; NK_IFN, IFN^{+}NK cells; NK_IL32.h, IL32^{high} NK cells; NK_NCAM1.h, NCAM1^{high} NK cells. (B)

NK cells from CENs exhibited increased percentages of granzyme B$^+$ cells compared with those from COs or CTs (Fig. 6B). No significant difference in the percentage of perforin 1–positive cells was seen across CENs, COs, and CTs (Fig. 6C).

NK cell cytotoxicity is tightly regulated by the balance between activating and inhibitory receptors on the membrane.[27] Therefore, we assessed changes in the mRNA expression levels of these receptors. As shown in Fig. 6D, the expressions of *KLRC1* [the gene encoding natural-killer receptor group 2, member A (NKG2A), an immune inhibitory receptor involved in self-nonself discrimination] and *KLRD1* (the gene encoding CD94, an immune receptor in self-nonself discrimination and microbial infection) in NK cells from CENs were increased compared with those in COs and CTs, while the expression of *KLRK1* [the gene coding natural-killer receptor group 2, member D (NKD2D), an activating and costimulatory receptor involved in immunosurveillance] was decreased in CENs compared with the expressions in COs and CTs. The expression patterns of these molecules were further analysed by flow cytometry. As shown in Fig. 6E, the percentage of NKG2A$^+$ cells was significantly decreased in PBMCs from CENs compared with the percentages in those from both COs and CTs ($P < 0.05$), which is completely opposite to the *KLRC1* mRNA expression patterns. Furthermore, the percentage of NKG2C$^+$ (an immune activating receptor involved in self–nonself discrimination, encoded by *KLRC2*) were not significantly different across CENs, COs, and CTs (Fig. 6F). Moreover, the percentage of CD94$^+$ cells in PBMCs was increased in CENs compared with that in CTs, but not in COs (Fig. 6G). The percentage of NKG2D$^+$ cells in PBMCs was increased in CENs compared with that in COs, but not in CTs (Fig. 6H).

Enhanced cell–cell interactions among NK and T cell subsets in centenarians compared with younger controls

Having defined the landscape of the main clusters of peripheral immune cells, we next investigated cell–cell interactions among key PBMC clusters. As seen in Fig. 7A and B, there were significant differences in cell–cell contact and secreted signals, especially between NK cells and T cell clusters. ECM (extracellular matrix)–receptor interactions among the PBMC clusters were difficult to detect (Fig. 7C). Enhanced cell–cell contacts were observed between NCAM1^{low}NK cells and IFN$^+$CD4$^+$ T cells, CD4$^+$Th2 cells, CD8$^+$CTL cells, HLA-DRs$^+$CD8$^+$ T cells, and GZMK$^+$CD8$^+$Tcm cells, while interactions between NCAM1^{high}NK cells and T cells were largely decreased (Fig. 7D). The MHC-I pathway was highly activated in NK cell and T cell subset interactions, especially in interactions between NK cells and CMC1$^+$CD8$^+$ T cells, CD8$^+$CTL cells, HLA-DRs$^+$CD8$^+$ T cells, CD8$^+$Tcm cells, and gdT cells. Most of the interactions were decreased, while enhanced interactions existed between NCAM1^{low}NK cells and CD8$^+$Tcm cells with regard to MHC-I signalling and NCAM1^{low}NK cells with CD4$^+$ and CD8$^+$ T cells with regard to CD99 signalling (Fig. 7E). Most of the cell contacts involving HLA molecules expressed by NCAM1^{high}NK cells, and CD8A/CD8B in CD8$^+$ T cell subsets were suppressed. In addition, we observed increased interactions between NCAM1^{low}NK cells and HLA-DRs$^+$CD8$^+$ T cells/CD8$^+$Tcm with regards to HLA-CD8A/B, between NCAM1^{low}NK cells and CD4$^+$ T cells with regards to HLA-CD4. Cell contacts involving CD99 signalling were enhanced among NCAM1^{low}NK cells and T cell subsets, promoting T cell adhesion (Supplementary Fig. S11A and B). Flow cytometry analysis showed that almost all CD56^{dim}NK cells were HLA-A/B/C positive, with no significant difference with regard to cell percentage and geometric mean fluorescence intensity (gMFI) in PBMCs across CENs, COs, and CTs (Fig. 7F), while the percentage of HLA-E$^+$ NK cells was significantly increased in PBMCs from CENs compared with the percentages of those from COs and CTs (Fig. 7G). Furthermore, the percentage of CD99$^+$ NK cells was significantly increased in PBMCs from CEN, compared with the percentages of those from both COs and CTs, while the percentage of CD99$^+$CD8$^+$ T cells in PBMCs was not significantly different among CENs, COs, and CTs (Supplementary Fig. S11C and D). These results indicated that NCAM1^{low}NK cells play dominant roles in antigen processing/presentation and T cell adhesion.

As for secreted signals, enhanced interactions existed between NCAM1^{low}NK cells and cytotoxic cells and

Expression of top expressed marker genes per cell subset. (C) Box plots showing the percentages of key subsets of NK and γδ T cells in CEN, CO, and CT groups by incorporating the scRNA-seq data of three cohorts. The percentages of cell subsets were presented as medians plus interquartile ranges. $N_{CEN} = 19$, $N_{CO} = 10$, and $N_{CT} = 15$. (D) UMAP plots of NK and γδ T cells with cell proportion density, dividing into CEN, CO and CT groups. (E) CyTOF analysis revealed the percentages of key NK cell subsets (CD56^{dim}CD16$^+$ and CD56^{bright}CD16$^-$) in CEN, CO and CT groups. The percentages of cell subsets were presented as medians plus interquartile ranges. $N_{CEN} = 9$, $N_{CO} = 6$, and $N_{CT} = 5$. (F to H) Key TF network analysis in NK cells (F), with the expression patterns and distribution analyses of these TFs in UMAPs (G) and violin plots (H). $N_{CEN} = 19$, $N_{CO} = 10$, and $N_{CT} = 15$. (I) Representative flow cytometry plots of RUNX3-expressing NK cells (left). Comparison of the frequency of RUNX3–expressing cells in CD56^{dim} NK cells in CEN, CO and CT groups (right). The percentages of cell subsets were presented as medians plus interquartile ranges. $N_{CEN} = 10$, $N_{CO} = 7$, and $N_{CT} = 7$. All the statistical significance was determined using the Kruskal–Wallis test followed by Dunn's multiple comparison tests. (*$P < 0.05$, **$P < 0.01$, ***$P < 0.001$, ****$P < 0.0001$, ns, not significant).

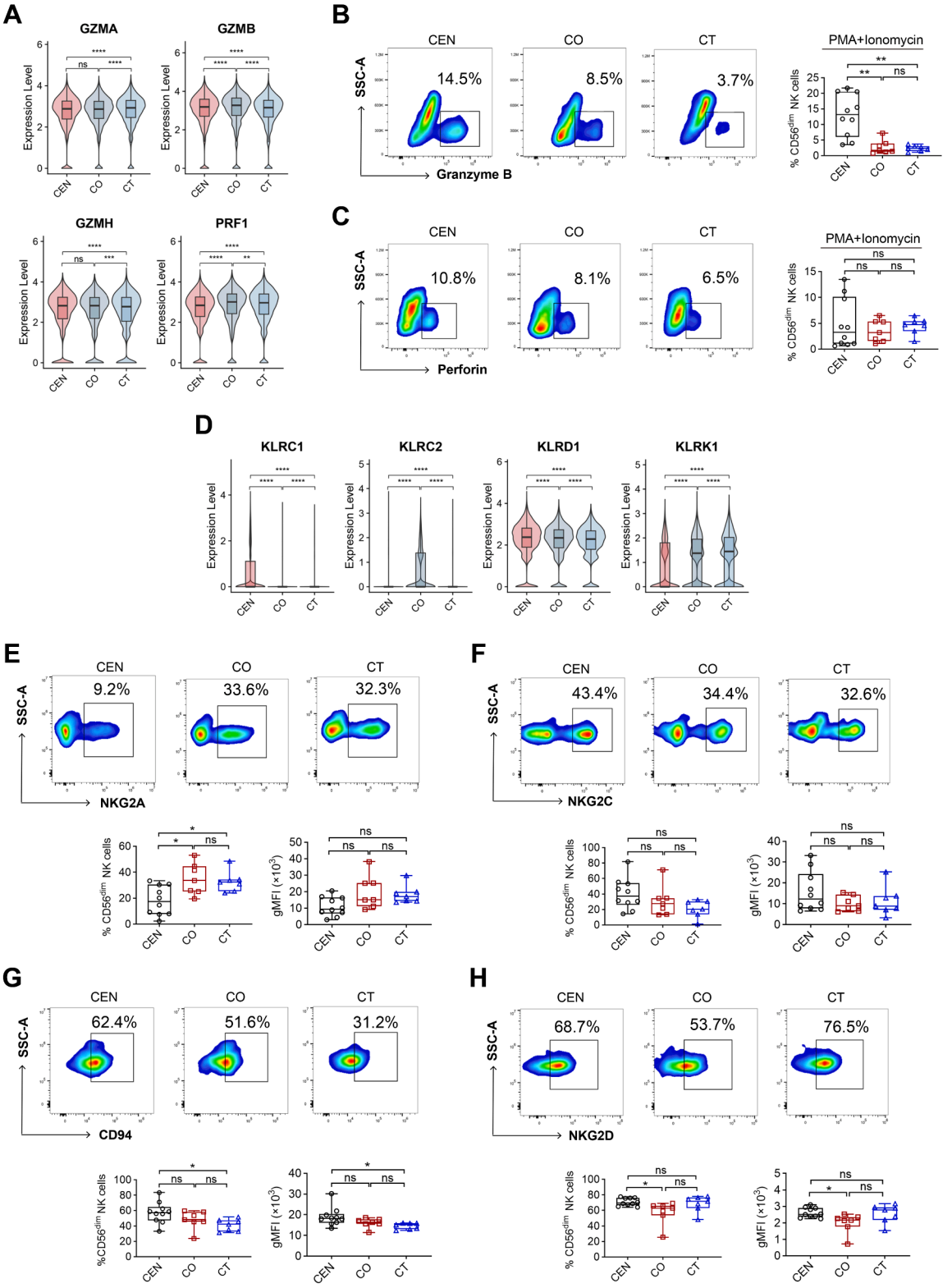

***Fig. 6:* NK cells from centenarians exhibit unique signatures compared with those in their younger controls**. (A) The violin plots showing the mRNA expression patterns of cytotoxic genes (*GZMA*, *GZMB*, *GZMH*, and *PRF1*) in NK cells across CEN, CO and CT groups. N_{CEN} = 19,

Tcm cells, while NCAM1^{high}NK cells interacted with a wide range of T cell subsets, including cytotoxic cells, CD4$^+$Th cells, and HLA-DRs$^+$CD8$^+$ T cells (Fig. 7H). Macrophage migration inhibitory factor (MIF) signalling was significantly upregulated in all these interactions, promoting the immune response and antimicrobial capacity (Fig. 7I, Supplementary Fig. S12A and B). Flow cytometry analysis showed that the percentage of CD74$^+$CD8$^+$ T cells in PBMCs from CENs was higher compared with that in those from COs, but not in those from CTs (Fig. 7J), and the percentage of CD44$^+$ NK cells in PBMCs was significantly upregulated in CENs compared with those in COs and CTs (Fig. 7K). On the contrary, both the percentages and gMFI values of CD74$^+$ NK cells and CD44$^+$CD8$^+$ T cells in PBMCs were not significantly different across CENs, COs, and CTs (Supplementary Fig. S12C and D). Furthermore, both the percentage and gMFI values of CXCR4$^+$ NK cells were significantly increased in PBMCs from CENs compared with those from CTs, but not in those from COs, while both the percentages and gMFI values of CXCR4$^+$CD8$^+$ T cells were lower in PBMCs from CENs compared with those from either COs or CTs (Supplementary Fig. S12E and F). Therefore, we demonstrated that enhanced MHC-I–associated antigen presentation and MIF interactions among NK cells and T cell subsets helps maintain the immune homoeostasis of PBMCs in CENs.

Discussion

Understanding immunological signatures is important for discovering the mechanisms underlying functional immune homoeostasis in centenarians. In this study, comprehensive single-cell omics analyses were conducted to analyse data from 17 CENs, 9 COs, and 14 CTs from the Lingao centenarian cohort, and scRNA-seq data from 14 CENs, 8 COs, and 12 CTs from the Rugao and Japanese centenarian cohorts were downloaded from public databases. Using scRNA-seq and CyTOF, we systematically analysed peripheral immune changes and detected decreased percentages of B cells and CD4$^+$T cells and increased percentage of NK cells in CENs. Specifically, increased percentages of CD4$^+$CTL cells, CMC1$^+$CD8$^+$T cells, CD8$^+$CTL cells, and TRGC$^+$ γδ T cells were observed in CENs compared with the findings in CTs. GSEA showed enhanced antigen processing/presentation, cytokine production, and antimicrobial signalling in the main PBMC cell clusters. Unexpectedly, NK cells from CENs showed similar subset percentages and expression patterns of key cytotoxic/membrane receptors compared with those from control subjects. RUNX3 upregulation might be responsible for the "young" signature of NK cells in CENs. Reinforced interactions between NK and T cells might promote T cell functions by modulating the MHC-I, CD99, and MIF pathways, promoting antigen processing/presentation, T cell adhesion, and the immune response. Therefore, our study defined the comprehensive immune landscape of CENs and elucidated a new mechanism of healthy immune ageing in this population.

The worldwide population of centenarians has greatly increased in recent years. Centenarians account for approximately 1 of 5000 individuals in Europe and exemplify successful and healthy ageing.[28] They not only display a much longer lifespan but also exhibit delayed onset or even avoidance of major age-related diseases, such as cardiovascular disorders, neurodegenerative diseases, severe infections, and cancer.[29] Therefore, studying centenarians is valuable for human longevity and combatting the effects of ageing. Multi-omics techniques provide new tools for investigating the detailed pathogenic mechanisms of diseases and phenomena. Immune changes in CENs have attracted the attention of medical scientists. In 2019, Hashimoto et al. reported a marked increase in CD4$^+$ CTLs as a signature of supercentenarians from Japan.[10] These CD4$^+$ CTLs extracted from supercentenarians produced IFN-γ and TNF-α upon ex vivo stimulation, functioning as cytotoxic cells in the immune response. Then, Dong et al. reported that CENs from Rugao City in China exhibited accumulation of GZMB$^+$ and CMC1$^+$ CD8 T cells, with PBMCs transitioning from a naïve phenotype to a cytotoxic phenotype.[11] Moreover, Karagiannis et al. demonstrated significant shifts from CD4$^+$ T to B cell populations, identifying cell type signatures and gene expression profiles associated with age-related changes, by enrolling centenarian subjects and younger controls from the United States.[12] Zhu et al. reported a scRNA-seq–based ageing clock model showing that PBMCs from CENs express more

N_{CO} = 10, and N_{CT} = 15. (B and C) Representative flow cytometry plots of granzyme B–expressing CD56^{bright} NK cells (B), and perforin–expressing CD56^{dim} NK cells (C). Comparison of the frequency of positive cells in CD56^{dim} NK cells in CEN, CO and CT groups in the right box plots. The percentages of cell subsets were presented as medians plus interquartile ranges. N_{CEN} = 10, N_{CO} = 7, and N_{CT} = 7. (D) The violin plots showing the mRNA expression patterns of key surface receptors (*KLRC1*, *KLRC2*, *KLRD1*, and *KLRK1*) in NK cells across CEN, CO and CT groups. N_{CEN} = 19, N_{CO} = 10, and N_{CT} = 15. (E to H) Representative flow cytometry plots of NKG2A–expressing CD56^{dim} NK cells (E), NKG2C–expressing CD56^{dim} NK cells (F), CD94–expressing CD56^{dim} NK cells (G), and NKG2D–expressing CD56^{dim} NK cells (H). Comparison of the percentages of positive cells and gMFI values in CD56^{dim} NK cells across CEN, CO and CT groups in the below box plots. The percentages and gMFI values were presented as medians plus interquartile ranges. N_{CEN} = 10, N_{CO} = 7, and N_{CT} = 7. All the statistical significance was determined using the Kruskal–Wallis test followed by Dunn's multiple comparison tests. (*P < 0.05, **P < 0.01, ****P < 0.0001, ns, not significant).

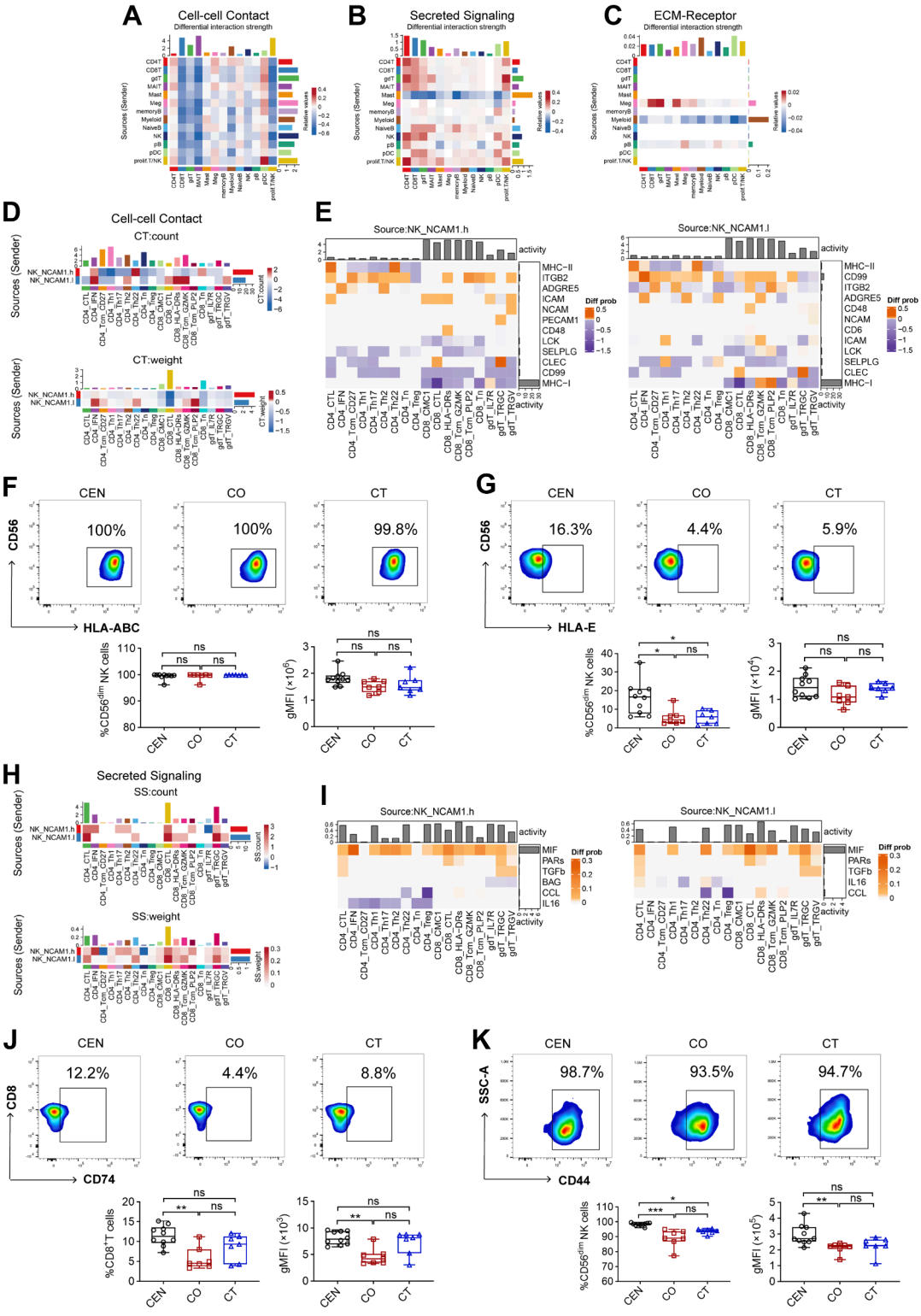

Fig. 7: **Cell–cell communications among key cell subsets across centenarians and their younger controls**. (A–C) Cell communication strength (cell–cell contact, secreted signalling, and ECM–receptor) among different cell clusters were plotted in heatmaps. Prolif. T/NK, proliferative T/NK cells. (D and E) The detailed interactions and pathways among NCAM1^{high} and NCAM1^{low} NK cells with T cell subset with

cell types with higher ribosome levels, contributing to low inflammation and a slow ageing status.[30] Additionally, advances in CyTOF help provide comprehensive information regarding the immune cell composition, phenotype, and function of peripheral blood and other tissues.[31] However, CyTOF has not been used to analyse the immune phenotypes of CENs. In this study, we collected single-cell omics data from CENs and control subjects from the Lingao centenarian cohort, the Rugao centenarian cohort,[11] and the Japanese centenarian cohort[10] to comprehensively analyse the peripheral immune status of CENs. Our results provide novel insights into changes in $CD4^+$ T cell, $CD8^+$ T cell, B cell, myeloid cell, and NK cell proportions and differentiation through TCR analysis, GSEA, TF network analysis, cell–cell contact analysis, and functional molecule expression analysis, providing a deeper understanding of the immune landscape of CENs and potential targets for treating or preventing immunosenescence.

Previous studies have demonstrated the effects of ageing on peripheral $CD4^+$ T cells, with decreased percentages of naïve $CD4^+$ T cells and interferon-activated subsets, decreased TCR clonotype richness, and an increased percentage of effector memory T cells (T_{EM} cells) in the blood.[32] Elyahu et al. demonstrated an accumulation of anti-inflammatory Treg cells and a marked expansion of cytotoxic $CD4^+$ T cells in ageing mice.[33] The increased percentage of $CD4^+$ CTLs was validated in supercentenarians by Japanese scientists using scRNA-seq.[10] Moreover, incomplete differentiation of aged $CD4^+$ T cells into Th1 and Th2 cells has been observed, while the ability of aged $CD4^+$ T cells to acquire a Th17 phenotype is not compromised in aged mice.[34] In our study, we found an increased percentage of $CD4^+$CTLs, and decreased $CD4^+$Tcm, $CD4^+$Tn, and $CD4^+$Th17 cell percentages in CENs, compared with the findings in CTs. Therefore, CENs not only exhibited higher numbers of $CD4^+$CTL cells, which maintain the immune response and antimicrobial capacity, but also a decreased percentage of Th17 cells, indicating a lower level of inflammageing.

Ageing-associated changes in $CD8^+$ T cells were similar to those seen in $CD4^+$ T cells, with decreased abundance of naïve cells, decreased TCR clonotype richness, and increased abundance of T_{EM} cells.[35] However, ageing is accompanied by decreased percentage of $CD8^+$ cytotoxic cells, as a marker of immune ageing,[1] while centenarians exhibited significantly increased percentages of $CD8^+$ CTLs both in our study and in Dong et al.'s study.[11] A multi-omics study demonstrated that, in healthy lean mice, the proportion of $GZMK^+$, but not $GZMB^+$, $CD8^+$ T_{EM} cells increased with age.[15] A mass cytometry study of an ageing cohort consisting of 156 healthy individuals confirmed these observations.[36] Another large-scale multi-omics study also reported changes of $GNLY^+CD8^+$ effector memory T cells and $CD8^+$ MAIT cells with increased age, by recruiting 220 healthy volunteers, spanning 13 age groups from 0 to over 90 years.[37] This study revealed that T cells were the most strongly affected by age, which provides with more insights of immune system ageing across the whole human lifespan. In our study, we demonstrated that the CENs exhibited increased percentages of $CD8^+$CTL and $CMC1^+CD8$ T cells and upregulated expression of cytotoxic markers. No significant changes were observed in percentages of $CD8^+$Tcm and $HLA\text{-}DRs^+CD8^+$ T cells across CENs, COs, and CTs. These findings are quite different from previous observations of immune ageing of $CD8^+$ T cells. Moreover, expression of the HLA class II histocompatibility antigens HLA-DRA and HLA-DQA1 was significantly upregulated in CENs compared with the expressions in COs and CTs. Therefore, $CD8^+$ T cell remodelling in CENs was directed preferentially to the cytotoxic and antigen processing/presentation branches to maintain healthy immune functions.

As for peripheral B cells, cell numbers and percentages decline significantly, and humoural immune responses against pathogens and vaccines are impaired.[7] We found that the percentage of B cells was significantly decreased in CENs compared with the percentage in their younger controls. Frasca et al. discovered that ageing affects peripheral B cells: aged murine plasma cells mainly secrete IgM, whereas young murine plasma cells mainly secrete IgG.[38] A previous study demonstrated that the proportion of ABCs, which are different from conventional naïve and memory B cells, increased.[39] A recent study has shown that ABCs arise from homoeostatic expansion to balance B cell progenitor loss.[40] Frasca et al. reported that ABCs can secrete pro-inflammatory cytokines but do not produce antibodies in response to influenza antigens in older individuals.[41] Therefore, ABCs are key

regard to cell–cell contact in heatmaps. (F and G) Representative flow cytometry plots of HLA-A/B/C–expressing $CD56^{dim}$ NK cells (F) and HLA-E–expressing $CD56^{dim}$ NK cells (G). Comparison of the percentages of positive cells and gMFI values in $CD56^{dim}$ NK cells across CEN, CO and CT groups in the below box plots. The percentages and gMFI values were presented as medians plus interquartile ranges. $N_{CEN} = 10$, $N_{CO} = 7$, and $N_{CT} = 7$. (H and I) The detailed interactions and pathways among $NCAM1^{high}$ and $NCAM1^{low}$ NK cells with T cell subsets with regard to secreted signalling using heatmaps. (J and K) Representative flow cytometry plots of CD74–expressing $CD8^+$ T cells (J) and CD44–expressing $CD56^{dim}$ NK cells (K). Comparison of the percentages of positive cells and gMFI values in $CD56^{dim}$ NK cells/$CD8^+$ T cells in CEN, CO and CT groups in the below box plots. The percentages and gMFI values were presented as medians plus interquartile ranges. $N_{CEN} = 10$, $N_{CO} = 7$, and $N_{CT} = 7$. All the statistical significance was determined using the Kruskal–Wallis test followed by Dunn's multiple comparison tests. (*P < 0.05, **P < 0.01, ***P < 0.001, ns, not significant).

players in the enhanced basal inflammatory states associated with immunosenescence.[7] However, because of the great heterogeneity of ABCs, their function is still controversial. Terekhova et al. used scRNA-seq to analyse age-associated changes in 166 healthy controls and found no significant changes in B cell subclusters.[17] In our study, we defined ABCs as Zinc finger E-box-binding homoeobox 2 (ZEB2)$^+$ PBMCs and found no significant difference in the percentage of ABCs in CENs compared with that in control subjects. Therefore, the lack of a significant change in ABCs may help explain the healthy immune balance in CENs, while in individuals with immunosenescence, targeting pro-inflammatory ABCs could be an attractive strategy to combat ageing-related immune disorders.

NK cells bridge the innate and adaptive immune system. Age-related changes in NK cells include a reduction in immature CD56^{bright} cells (immunoregulatory) and an accumulation of highly differentiated CD56^{dim}CD57$^+$ NK cells (cytotoxic).[35] Ageing-associated changes in NK cells include reduced perforin-mediated cytotoxicity and cytokine/chemokine production, resulting in accumulation of senescent cells, reduced anti-viral immunity, and reduced anti-microbial immunity.[42] Also, changes in NK cell surface marker phenotypes have additional consequences for the health of older adults.[42] scRNA-seq analysis of immune cells from the spleen, lung, and liver showed decreased NK cell abundance in older mice.[15] In the 1990s, Sansoni et al. reported that NK cells from CENs exhibited exceptionally well-preserved cytotoxicity.[43] However, they did not investigate the distribution and function of NK cell subsets in CENs. In this study, we observed an increased percentage of NK cells in PBMCs from CENs compared with that in those from CTs, via scRNA-seq and CyTOF analyses. Moreover, NK cells from CENs exhibited similar cell subset distribution and antimicrobials/cytokine receptor functions to those from control subjects. Upon cell stimulation cocktail activation, NK cells from CENs exhibited an increased percentage of granzyme B$^+$ cells compared with those from either COs or CTs, indicating well-preserved cellular cytotoxicity.

Importantly, NK cell activity is tightly controlled through a variety of stimulatory, co-stimulatory, and inhibitory receptors. In humans, the HLA class I receptors include killer cell Ig-like receptors that recognise HLA-A, -B, and -C epitopes and CD94:NKG2A heterodimers that recognise HLA-E.[44] Among these membrane receptors, CD94 is a member of the C-type lectin receptor family, which forms heterodimers with several members of the NKG2 family.[45] CD94/NKG2A functions as an inhibitory receptor, while CD94/NKG2C and NKG2D trigger NK cell effector activity and function.[46] In our detailed analysis of PBMCs using flow cytometry, we demonstrated that the percentage of NKG2A$^+$ NK cells was significantly decreased, with the percentage of CD94$^+$ NK cells significantly increased, in CENs compared with the findings in COs and CTs, which partially contributed to the enhanced cytotoxicity of NK cells from CENs. In human studies, CD94 has been linked to improved antiviral responses and NK cell development,[47] which is also associated with adaptive NK cell responses, likely because of its physical interaction/formation of a heterodimer with NKG2C.[48] The CD94/NKG2A complex functions as an immune checkpoint and an important target for cancer immunotherapy.[49]

TFs are essential for the development, maturation, and function of different lineages of PBMCs in that they alter gene expression patterns by binding to specific genomic sites and alter chromatin states, leading to cell type identity changes.[50] Recent studies have also revealed that ageing-related changes in immune phenotypes are regulated by certain TFs.[51] Dong et al. reported that the EOMES, JUND, and ATF3 regulatory network is strongly associated with immune homoeostasis in CENs.[11] By analysing CD4$^+$ T cells regulatory networks, we demonstrated that RUNX3, NFATC2, and LEF1 cooperatively maintain immune homoeostasis in CENs. As for NK cells, RUNX3, KLF4, and FOS upregulation might play a dominant role in cell development and function. More importantly, we further validated the upregulation of RUNX3 expression in CD4$^+$ T cells and NK cells from CENs, compared with that in those from CTs. Previous studies have demonstrated the key role of RUNX3 in NK cell activation and cytotoxicity,[52] CD4$^+$ T cell function,[53] and CD8$^+$ T cells tissue residency.[54] Moreover, RUNX3 is an important component of the transcriptional regulation of effector CTL cells.[55] Therefore, further studies are essential to further identify the role and regulatory patterns of these TFs in maintaining immune homoeostasis in CENs.

Interactions among immune cells or immune cells and other cell types have been investigated widely using single-cell transcriptomic data.[56] Regarding NK cells, previous studies have mainly concentrated on interactions between NK cells and myeloid cells (monocytes, macrophages, MDSCs, DCs), tumour cells, and platelets.[57] Interactions between NK cells and Tregs lead to NK cell suppression, in particular impairing NK cell effector functions.[58] In this study, we revealed that NK cells interacted with several T cell subsets, possibly via the MHC-1 pathway, to facilitate antigen presentation and MIF signalling to promote lymphocyte activation, using the scRNA-seq data. Generally, NK cells are not considered typical antigen processing cells (APCs), while adaptive NK cells may activate CD4$^+$ T cells or CD8$^+$ T cells via antigen processing.[59] By predicting cell–cell contacts, we revealed that MHC-I class molecule–CD8 interactions were enhanced among the CD56^{dim} NK cells and CD8$^+$ T cell subsets. Using flow cytometry, we further validated this observation, showing that the percentage of HLA-E$^+$NK cells was

increased in CENs compared with the percentages in either COs or CTs. MIF signalling is reported to primarily function in not only cell ageing, but also in antimicrobial and cytokine production.[60] We further validated the expression patterns of these molecules via flow cytometry. Therefore, an increased percentage of relatively "young" NK cells in CENs maintains innate immune function and promotes adaptive immunity.

The limitations of the study are as follows: first, the sample size is still small, especially for CyTOF and flow cytometry experiments; second, the regulatory patterns and functions of key TFs still need further investigation.

In conclusion, we identified the unique immune signatures of CENs by analysing data from three centenarian cohort using multi-omics techniques. Immune cells from CENs showed enhanced cytotoxicity, cytokine production, and antigen presentation capacity. Increased proportions of NK cells with relatively young immune signatures interacted with T cell subsets and promoted T cell functions by modulating MHC-I, CD99, and MIF signals. Taken together, these findings increase our understanding of the unique immune mechanisms of healthy ageing, while providing strategies for intervention in age-related immune disorders to facilitate healthy ageing.

Contributors

Conceptualisation: Yizhi Chen, Zhifeng Gu, and Xiangmei Chen.

Data curation: Bin Wang, and Zehao Zhang.

Formal analysis: Bin Wang, Zehao Zhang, Qing Ouyang, and Min Zhang.

Funding acquisition: Yizhi Chen, Zhifeng Gu, and Xiangmei Chen.

Investigation: Bin Wang, Zehao Zhang, Qing Ouyang, Min Zhang, Mingda Duan, and Hongyan Hu.

Methodology: Bin Wang, Zehao Zhang, Qing Ouyang, Min Zhang, Mingda Duan, Hongyan Hu, Qingtao Zhang, Xinye Jin, Jie Zhang, Qing Luo, Ding Sun, Hao Li, and Zeyu Qu.

Project administration: Yizhi Chen, Zhifeng Gu, and Xiangmei Chen.

Resources: Mingda Duan, Hongyan Hu, Qingtao Zhang, Xinye Jin, Jie Zhang, Qing Luo, Ding Sun, Hao Li, and Zeyu Qu.

Software: Bin Wang, Zehao Zhang, Qing Ouyang, and Min Zhang.

Supervision: Yizhi Chen, Zhifeng Gu, and Xiangmei Chen.

Validation: Yizhi Chen, Zhifeng Gu, and Xiangmei Chen.

Visualisation: Bin Wang, Zehao Zhang, Qing Ouyang, Min Zhang, and Yizhi Chen.

Writing—original draft: Bin Wang, and Zehao Zhang.

Writing—review & editing: Yizhi Chen, Zhifeng Gu, and Xiangmei Chen.

Authors have directly accessed and verified data reported in the manuscript: Bin Wang, Zehao Zhang, Yizhi Chen, Zhifeng Gu, and Xiangmei Chen.

All authors contributed substantially to the study design, data analysis, or interpretation. All authors reviewed the manuscript for intellectual content, contributed to revisions, and approved the final version for submission.

Data sharing statement

The dataset generated and analysed in the current study are available from the corresponding author on reasonable request. Data is deposited in the Genome Sequence Archive for Human (https://ngdc.cncb.ac.cn/gsa-human/) under the accession number HRA011570.

Declaration of interests

The authors declare no competing interests.

Acknowledgements

We sincerely thank Suzhou Lingdian Biotechnology Co., Ltd. for their technical support and assistance in scRNA-seq data analysis. We thank Dr. Lu Jia from Capital Medical University, and Dr. Chen Dong from Nantong University in the guidance of data analysis in scRNA-seq and flow cytometry, Dr. Xiuyun Ren and Mrs. Qiushi Wang from Hainan Hospital of Chinese PLA General Hospital in collecting human specimens during manuscript revision. We also thank Dr. Weiguang Zhang, Dr. Zhe Feng, and Dr. Guangyan Cai, all from Chinese PLA General Hospital, in revising and improving the discussion section. We appreciated for the centenarians and healthy participants who volunteered to participate in this study.

This study was funded by the Sanya Science and Technology Innovation Special Project (No. 2022KJCX02), National Natural Science Foundation of China (No. 32141005, 82270769), Specific Research Fund of the Innovation Platform for Academicians of Hainan Province, and National Key Research and Development Program of China (No. 2022YFC3602900, 2022YFC3602902, 2022YFC3602903).

Appendix A. Supplementary data

Supplementary data related to this article can be found at https://doi.org/10.1016/j.ebiom.2025.105922.

References

1 Borgoni S, Kudryashova KS, Burka K, de Magalhães JP. Targeting immune dysfunction in aging. *Ageing Res Rev*. 2021;70:101410.
2 Chang AY, Skirbekk VF, Tyrovolas S, Kassebaum NJ, Dieleman JL. Measuring population ageing: an analysis of the global burden of disease study 2017. *Lancet Public Health*. 2019;4(3):e159–e167.
3 Kennedy BK, Berger SL, Brunet A, et al. Geroscience: linking aging to chronic disease. *Cell*. 2014;159(4):709–713.
4 Liu Z, Liang Q, Ren Y, et al. Immunosenescence: molecular mechanisms and diseases. *Signal Transduct Target Ther*. 2023;8(1):200.
5 Yousefzadeh MJ, Flores RR, Zhu Y, et al. An aged immune system drives senescence and ageing of solid organs. *Nature*. 2021;594(7861):100–105.
6 Goronzy JJ, Weyand CM. Mechanisms underlying T cell ageing. *Nat Rev Immunol*. 2019;19(9):573–583.
7 Cancro MP. Age-associated B cells. *Annu Rev Immunol*. 2020;38:315–340.
8 Gayoso I, Sanchez-Correa B, Campos C, et al. Immunosenescence of human natural killer cells. *J Innate Immun*. 2011;3(4):337–343.
9 Wang Y, Dong C, Han Y, Gu Z, Sun C. Immunosenescence, aging and successful aging. *Front Immunol*. 2022;13:942796.
10 Hashimoto K, Kouno T, Ikawa T, et al. Single-cell transcriptomics reveals expansion of cytotoxic CD4 T cells in supercentenarians. *Proc Natl Acad Sci U S A*. 2019;116(48):24242–24251.
11 Dong C, Miao YR, Zhao R, et al. Single-cell transcriptomics reveals longevity immune remodeling features shared by centenarians and their offspring. *Adv Sci (Weinh)*. 2022;9(36):e2204849.
12 Karagiannis TT, Dowrey TW, Villacorta-Martin C, et al. Multimodal profiling of peripheral blood cells across the human lifespan reveals distinct immune cell signatures of aging and longevity. *eBioMedicine*. 2023;90:104514.
13 Yang S, Corbett SE, Koga Y, et al. Decontamination of ambient RNA in single-cell RNA-Seq with DecontX. *Genome Biol*. 2020;21(1):57.
14 Stuart T, Butler A, Hoffman P, et al. Comprehensive integration of single-cell data. *Cell*. 2019;177(7):1888–1902.e21.
15 Mogilenko DA, Shpynov O, Andhey PS, et al. Comprehensive profiling of an aging immune system reveals clonal GZMK(+) CD8(+) T cells as conserved hallmark of inflammaging. *Immunity*. 2021;54(1):99–115.e12.
16 Tran HTN, Ang KS, Chevrier M, et al. A benchmark of batch-effect correction methods for single-cell RNA sequencing data. *Genome Biol*. 2020;21(1):12.
17 Terekhova M, Swain A, Bohacova P, et al. Single-cell atlas of healthy human blood unveils age-related loss of NKG2C(+)GZMB(-)CD8(+) memory T cells and accumulation of type 2 memory T cells. *Immunity*. 2023;56(12):2836–2854.e9.

18 Su M, Pan T, Chen QZ, et al. Data analysis guidelines for single-cell RNA-Seq in biomedical studies and clinical applications. *Mil Med Res*. 2022;9(1):68.
19 Street K, Risso D, Fletcher RB, et al. Slingshot: cell lineage and pseudotime inference for single-cell transcriptomics. *BMC Genomics*. 2018;19(1):477.
20 Ma Y, Sun S, Shang X, Keller ET, Chen M, Zhou X. Integrative differential expression and gene set enrichment analysis using summary statistics for scRNA-seq studies. *Nat Commun*. 2020;11(1):1585.
21 Jin S, Guerrero-Juarez CF, Zhang L, et al. Inference and analysis of cell-cell communication using CellChat. *Nat Commun*. 2021;12(1):1088.
22 Van de Sande B, Flerin C, Davie K, et al. A scalable SCENIC workflow for single-cell gene regulatory network analysis. *Nat Protoc*. 2020;15(7):2247–2276.
23 Finck R, Simonds EF, Jager A, et al. Normalization of mass cytometry data with bead standards. *Cytometry A*. 2013;83(5):483–494.
24 Samusik N, Good Z, Spitzer MH, Davis KL, Nolan GP. Automated mapping of phenotype space with single-cell data. *Nat Methods*. 2016;13(6):493–496.
25 Jamieson AR, Giger ML, Drukker K, Li H, Yuan Y, Bhooshan N. Exploring nonlinear feature space dimension reduction and data representation in breast Cadx with Laplacian eigenmaps and t-SNE. *Med Phys*. 2010;37(1):339–351.
26 Ren X, Wen W, Fan X, et al. COVID-19 immune features revealed by a large-scale single-cell transcriptome atlas. *Cell*. 2021;184(7):1895–1913.e19.
27 Kyrysyuk O, Wucherpfennig KW. Designing cancer immunotherapies that engage T cells and NK cells. *Annu Rev Immunol*. 2023;41:17–38.
28 Borras C, Ingles M, Mas-Bargues C, et al. Centenarians: an excellent example of resilience for successful ageing. *Mech Ageing Dev*. 2020;186:111199.
29 Cai Y, Song W, Li J, et al. The landscape of aging. *Sci China Life Sci*. 2022;65(12):2354–2454.
30 Zhu H, Chen J, Liu K, et al. Human PBMC scRNA-seq-based aging clocks reveal ribosome to inflammation balance as a single-cell aging hallmark and super longevity. *Sci Adv*. 2023;9(26):eabq7599.
31 Levine LS, Hiam-Galvez KJ, Marquez DM, et al. Single-cell analysis by mass cytometry reveals metabolic states of early-activated CD8(+) T cells during the primary immune response. *Immunity*. 2021;54(4):829–844.e5.
32 Mogilenko DA, Shchukina I, Artyomov MN. Immune ageing at single-cell resolution. *Nat Rev Immunol*. 2022;22(8):484–498.
33 Elyahu Y, Hekselman I, Eizenberg-Magar I, et al. Aging promotes reorganization of the CD4 T cell landscape toward extreme regulatory and effector phenotypes. *Sci Adv*. 2019;5(8):eaaw8330.
34 Maue AC, Eaton SM, Lanthier PA, Sweet KB, Blumerman SL, Haynes L. Proinflammatory adjuvants enhance the cognate helper activity of aged CD4 T cells. *J Immunol*. 2009;182(10):6129–6135.
35 Santoro A, Bientinesi E, Monti D. Immunosenescence and inflammaging in the aging process: age-related diseases or longevity? *Ageing Res Rev*. 2021;71:101422.
36 Arthur L, Esaulova E, Mogilenko DA, et al. Cellular and plasma proteomic determinants of COVID-19 and non-COVID-19 pulmonary diseases relative to healthy aging. *Nat Aging*. 2021;1(6):535–549.
37 Wang Y, Li R, Tong R, et al. Integrating single-cell RNA and T cell/B cell receptor sequencing with mass cytometry reveals dynamic trajectories of human peripheral immune cells from birth to old age. *Nat Immunol*. 2025;26(2):308–322.
38 Han S, Yang K, Ozen Z, et al. Enhanced differentiation of splenic plasma cells but diminished long-lived high-affinity bone marrow plasma cells in aged mice. *J Immunol*. 2003;170(3):1267–1273.
39 Dai D, Gu S, Han X, et al. The transcription factor ZEB2 drives the formation of age-associated B cells. *Science*. 2024;383(6681):413–421.
40 Swain SL, Kugler-Umana O, Kuang Y, Zhang W. The properties of the unique age-associated B cell subset reveal a shift in strategy of immune response with age. *Cell Immunol*. 2017;321:52–60.
41 Frasca D, Diaz A, Romero M, Thaller S, Blomberg BB. Metabolic requirements of human pro-inflammatory B cells in aging and obesity. *PLoS One*. 2019;14(7):e0219545.
42 Hazeldine J, Lord JM. The impact of ageing on natural killer cell function and potential consequences for health in older adults. *Ageing Res Rev*. 2013;12(4):1069–1078.
43 Sansoni P, Brianti V, Fagnoni F, et al. NK cell activity and T-lymphocyte proliferation in healthy centenarians. *Ann N Y Acad Sci*. 1992;663:505–507.
44 Parham P. MHC class I molecules and KIRs in human history, health and survival. *Nat Rev Immunol*. 2005;5(3):201–214.
45 Lanier LL. NK cell receptors. *Annu Rev Immunol*. 1998;16:359–393.
46 López-Botet M, Llano M, Navarro F, Bellón T. NK cell recognition of non-classical HLA class I molecules. *Semin Immunol*. 2000;12(2):109–119.
47 Fang M, Orr MT, Spee P, Egebjerg T, Lanier LL, Sigal LJ. CD94 is essential for NK cell-mediated resistance to a lethal viral disease. *Immunity*. 2011;34(4):579–589.
48 Orr MT, Wu J, Fang M, et al. Development and function of CD94-deficient natural killer cells. *PLoS One*. 2010;5(12):e15184.
49 Liu X, Song J, Zhang H, et al. Immune checkpoint HLA-E:CD94-NKG2A mediates evasion of circulating tumor cells from NK cell surveillance. *Cancer Cell*. 2023;41(2):272–287.e9.
50 Hosokawa H, Rothenberg EV. How transcription factors drive choice of the T cell fate. *Nat Rev Immunol*. 2021;21(3):162–176.
51 Goto M, Takahashi H, Yoshida R, et al. Age-associated CD4(+) T cells with B cell-promoting functions are regulated by ZEB2 in autoimmunity. *Sci Immunol*. 2024;9(93):eadk1643.
52 Lai CB, Mager DL. Role of runt-related transcription factor 3 (RUNX3) in transcription regulation of natural cytotoxicity receptor 1 (NCR1/NKp46), an activating natural killer (NK) cell receptor. *J Biol Chem*. 2012;287(10):7324–7334.
53 Reis BS, Rogoz A, Costa-Pinto FA, Taniuchi I, Mucida D. Mutual expression of the transcription factors Runx 3 and ThPOK regulates intestinal CD4$^+$ T cell immunity. *Nat Immunol*. 2013;14(3):271–280.
54 Milner JJ, Toma C, Yu B, et al. Runx 3 programs CD8(+) T cell residency in non-lymphoid tissues and tumours. *Nature*. 2017;552(7684):253–257.
55 Cruz-Guilloty F, Pipkin ME, Djuretic IM, et al. Runx3 and T-box proteins cooperate to establish the transcriptional program of effector CTLs. *J Exp Med*. 2009;206(1):51–59.
56 Armingol E, Officer A, Harismendy O, Lewis NE. Deciphering cell-cell interactions and communication from gene expression. *Nat Rev Genet*. 2021;22(2):71–88.
57 You J, Wang S, Zhu Y, et al. Natural killer cells reprogram myeloid-derived suppressor cells to induce TNF-α release via NKG2D-ligand interaction after cryo-thermal therapy. *Int J Mol Sci*. 2024;25(10):5151.
58 Pedroza-Pacheco I, Madrigal A, Saudemont A. Interaction between natural killer cells and regulatory T cells: perspectives for immunotherapy. *Cell Mol Immunol*. 2013;10(3):222–229.
59 Erokhina SA, Streltsova MA, Kanevskiy LM, Grechikhina MV, Sapozhnikov AM, Kovalenko EI. HLA-DR-expressing NK cells: effective killers suspected for antigen presentation. *J Leukoc Biol*. 2021;109(2):327–337.
60 Sumaiya K, Langford D, Natarajaseenivasan K, Shanmughapriya S. Macrophage migration inhibitory factor (MIF): a multifaceted cytokine regulated by genetic and physiological strategies. *Pharmacol Ther*. 2022;233:108024.